HIGHLY BIREFRINGENT, FLATTENED DISPERSION, LOW LOSS PCFS FOR THZ WAVE PROPAGATION

A thesis submitted to
Department of Electrical, Electronic and Communication Engineering
Military Institute of Science and Technology (MIST)
In partial fulfillment of requirement for the degree of
Bachelor of Science in Electrical, Electronic and Communication Engineering

By

Md. Sadman Mallick	Student ID: 201416013
M. Ahasanul Siam	Student ID: 201416058
Shahariar M. Sakib	Student ID: 201416060

Supervised by

Dr. Mohammad Faisal

Professor

Department of Electrical and Electronic Engineering

Bangladesh University of Engineering and Technology

Department of Electrical, Electronic and Communication Engineering

Military Institute of Science and Technology

December 2017

APPROVAL CERTIFICATE

The thesis titled "**Highly Birefringent, Flattened Dispersion, Low Loss PCFs for THz Wave Propagation**" submitted by **Md. Sadman Mallick, Student ID: 201416013, M. Ahasanul Siam, Student ID: 201416058 and Shahariar M. Sakib, Student ID: 201416060** Session 2013-14 has been accepted as satisfactory in partial fulfillment of the requirement for the degree of BACHELOR OF SCIENCE IN ELECTRICAL ELECTRONIC & COMMUNICATION ENGINEERING on 26 December, 2017.

DR. MOHAMMAD FAISAL (SUPERVISOR)
PROFESSOR
DEPARTMENT OF ELECTRICAL AND ELECTRONIC ENGINEERING
BANGLADESH UNIVERSITY OF ENGINEERING AND TECHNOLOGY
DHAKA-1205, BANGLADESH
PHONE: +88-02-55167100, 6168 (O), 01926714764 (M)
EMAIL: mdfaisal@eee.buet.ac.bd

CANDIDATES' DECLARATION

It is hereby declared that this thesis or any part of it has not been submitted elsewhere for the award of any degree or diploma and that all sources are acknowledged.

Signature of the Candidates:

1. _____

Md. Sadman Mallick

2. _____

M. Ahasanul Siam

3. _____

Shahariar M. Sakib

DEDICATION

To our respected parents

ACKNOWLEDGEMENT

First of all, we would like to thank Allah for giving us the ability to complete this thesis work.

We would like to express our utmost gratitude towards our honorable supervisor, Dr. Mohammad Faisal, without whose encouragement and guidance, this thesis would have never been completed. We are very grateful for his continuous instructions and encouragement, valuable discussions and careful review during the entire duration of the research. His thoughtful analyses and firm supervision have provided us with the right direction towards our goal. We have learned many valuable concepts of Optical fiber Communication from him throughout our study, which we tried to utilize and develop our analyzing abilities. His constant encouragement gave us the confidence to carry out our work.

We would also like to thank all our teachers. They gave the knowledge and directions needed throughout my life. We express our gratitude towards our teachers from Military Institute of Science and Technology (MIST). I want to thank my friends for providing me support and encouragement. Their suggestions helped me in countless ways.

Last but not the least, we would like to thank our parents. Their unconditional support made it possible to finish this thesis.

ABSTRACT

Photonic crystal fiber (PCF) is one kind of optical fiber having a number of air holes arranged in a crystal running longitudinally in its structure. It plays vital role in fiber optic communication systems where extensive research has been done for the past few years. THz electromagnetic transmission (0.1-10 THz) has been an area of increasing interest and extensive research over the past few years. PCFs have shown promising applications in THz transmission domain due to their design flexibility and simultaneous air-solid guiding mechanism.

In this thesis, different properties of PCF like dispersion, birefringence, confinement loss, power fraction etc. are investigated numerically by a full vectorial FEM. Two porous core octagonal photonic crystal fiber (PCF) for terahertz (THz) wave propagation are proposed in our thesis. One of the design is highly birefringent photonic crystal fiber (PCF) with all circular holes for transmission in the terahertz (THz) regime. It shows a very high birefringence about 0.045 at 1 THz and flattened dispersion of 2.2 ± 0.09 ps/THz/cm within 0.7 THz to 0.95 THz. And the other design exhibits low loss properties. A very low material absorption loss ($0.076 cm^{-1}$) and low confinement loss ($0.0006 cm^{-1}$) are obtained from the proposed design. This two designs are expected to be useful for efficient transmission of broadband terahertz radiation.

TABLE OF CONTENTS

TABLE OF FIGURES

LIST OF ABBREVIATIONS

PCF: Photonic Crystal Fiber

TIR: Total Internal Reflection

M-TIR: Modified Total Internal Reflection

MOF: Micro-structured Optical Fiber

PBG: Photonic Band Gap

ESM: Endlessly Single Mode

SCG: Super Continuum Generation

OSA: Optical Spectrum Analyzer

OCT: Optical Coherence Tomography

SCF: Suspended Core Fiber

FEM: Finite Element Method

PML: Perfectly Matched Layer

GVD: Group Velocity Dispersion

ZWD: Zero Wavelength Dispersion

WDM: Wavelength Division Multiplexing

DFB: Distributed Feedback

FWM: Four Wave Mixing

SPM: Self Phase Modulation

XPM: Cross Phase Modulation

DCF: Dispersion Compensating Fiber

DSF: Dispersion Shifted Fiber

LIST OF SYMBOLS

N : Refractive Index

α : Attenuation Constant

β : Propagation Constant

γ : Nonlinear Parameter

D : Dispersion

D_M : Material Dispersion

D_W : Waveguide Dispersion

Λ : Lattice Constant

d : Diameter of Air-Hole

ω: Angular Frequency

λ : Wavelength

E: Electric field

H: Magnetic Field

σ_e: Electric conductivity of PML

σ_m: Magnetic conductivity of PML

Chapter 01
Introduction

Optical fibers have undergone an evolution in its structure since they were first introduced in the beginning of 1970s as step index fibers. Photonic crystal fibers (PCFs) are a special type of optical fiber. Conventional optical fibers can only guide light in a high refractive index core by total internal reflection. By using total internal reflections, it is not possible to guide light in an air core. Light guidance in air is of great interest for various technological and scientific applications and has only recently been possible with the advent of photonic band gap fibers. PCFs guide light by two mechanisms. One is the modified total internal reflection that utilizes its microstructured cladding arrangement and solid core and the other is the photonic band gap mechanism in PCFs having hollow cores. In recent days, intense interesting has focused on terahertz (THz) spectrum ranging from 0.1 to 10 THz as this band of frequency has so many promising and potential applications expanding from traditional fields of astronomy to new fields. The numerous structural parameters can be tailored to obtain desirable values of dispersion, birefringence, confinement loss bending loss etc for particular applications.

1.1 Background of Photonic Crystal Fiber:

Photonic Crystal Fiber (PCF) also known as microstructure optical fiber or holey fiber is a kind of advanced optical fiber technology [1]. It is a great recent research-field for optical engineering due to the additional purposes it serves unlike conventional optical fibers.

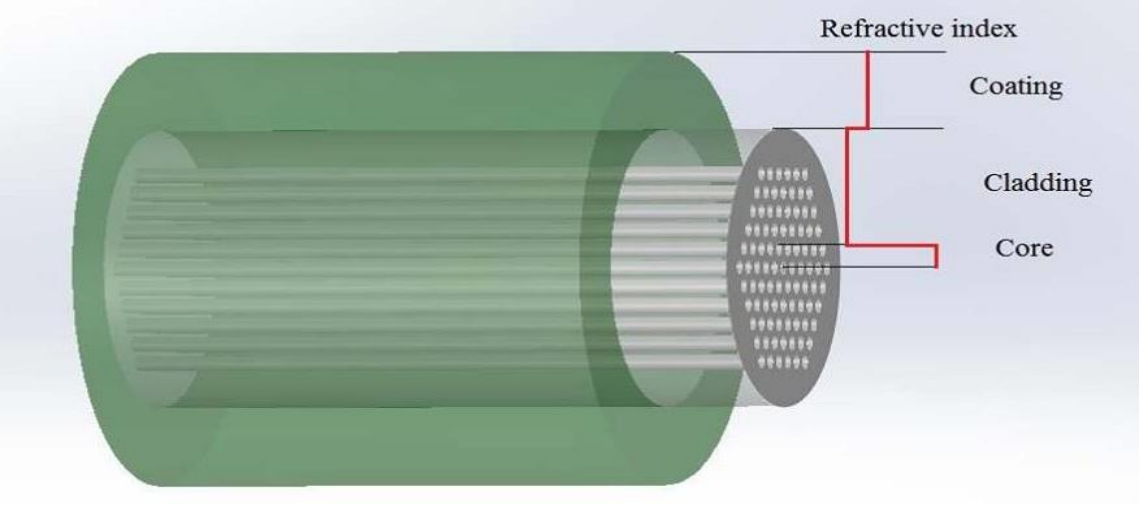

Fig. 1.1: Cross Section of Photonic Crystal Fiber (PCF)

These fibers can guide light by means of total internal reflection, as in standard fibers, or by the photonic band gap effect. There also exist fibers with a periodicity in the propagation

direction of the light. Such fibers are called fiber gratings. The axial periodicity can induce coupling of light between co-propagating or counter-propagating modes.

1.2 Initial Developments of PCF:

From the early research, it is found that light may behave quite similarly as electron waves in crystal lattice. The periodic potentials in crystal create a frequency band in which the propagation of electron waves of certain energies is prohibited. This frequency band in photonic crystals is called photonic band gap (PBG) [2]. Photonic crystal is a low-loss periodic dielectric medium containing a periodic array of microscopic air-holes that run along the total fiber length. From the introduction of conventional step index fiber in 1970, the researchers led the way for photonic crystals as a more efficient mode of fiber-optics since 1987.Fiber-optic cables are constructed with a core and a cladding of constant refractive index difference. Light travels through the core as a result of the refraction property of light, which occurs as a result of the difference between the refractive indexes of the core and cladding. This refracted light bears much higher loss during propagation over extended distances, and therefore it requires repeaters and amplifiers for extended distance communications in recent days.

The main physical differences of PCF from the conventional fiber is that PCF contains air-holes all through the length. The core diameter is another unique property of PCF where it is kept as less as possible for nonlinear propagation of light. As a matter of fact, PCFs may be considered a subgroup of a more general class of micro structured optical fibers. And in PCFs, light is guided by structural modification as well as refractive index difference whereas conventional fiber optics only deals with refractive index difference [3]. PCF can also be made from a single material and have several geometric parameters which can be manipulated offering large flexibility in design.

After the invention of Ruby Laser by Mainman in 1960, optics turned into photonics [4]. The lasers offered coherent radiation and short pulses, something that was unavailable in classical optics. This led to a revolution in many fields such as nonlinear optics, telecommunications, atomic and molecular spectroscopy and biology.Besides, it is to be noted that, the continuous progress during the last decade in the fabrication of photonic nanostructures results one, two and three-dimensional periodic structures made of materials with different dielectric constant.

Periodic potentials in a semiconductor crystal affect the motion of electron by defining forbidden and allowed electronic energy band from the band theory of electrons and photonic crystals works in the same way for electromagnetic waves. The microstructure creates a boundary for the photons to pass through depending on wavelength. The wavelengths that

propagate are called modes and groups of allowed modes form bands. The bands that are not allowed are called photonic band gaps. Therefore it is also known as 'semiconductor of light'.

In silicon and other semiconductors, adjacent atoms are separated by about a quarter of a nanometer. Photonic band gap materials involve similar structures but at larger scales. A typical example would be a block of glass with a closely spaced array of cylindrical holes. Let us consider each hole with a diameter of 400 nanometers. So these openings are analogous to the atoms in a semiconductor. Mostly the spacing of the array is reasonably close to the wavelength of the light or the electromagnetic waves to be controlled.

Light entering the holey material will refract through and partially reflect off the internal interfaces between air and glass. The complex pattern of overlapping beams will reinforce or cancel one another out according to the light's wavelength, its direction of travel through the crystal, the refractive index of the glass, and the size and arrangement of all the holes in the fiber. Perfect cancellation in all directions for a narrow band of wavelengths is like the band gap for electrons in semiconductors: that band of light cannot propagate through the crystal. A photonic crystal is mostly made of an electronic semiconductor material, and so the crystal has both an electronic band gap and a photonic band gap.

1.3 Application of PCF:

After the first experimental demonstration of PCF in 1996, the optical properties and fabrication of this type of fiber have attract very high attention because of its vast application. The physical application of PCF are many, in them some of the application are discussed below.

1.3.1 Supercontinuum Generation:

Supercontinuum (SC) generation is the formation of broad continuous spectra by propagation of high power pulses through nonlinear media, and was first observed in 1970 by Alfano and Shapiro. The term SC does not cover a specific phenomenon but rather a plethora of nonlinear effects, which, in combination, lead to extreme pulse broadening [5].

The most straight-forward application for SC sources is a replacement for the common, and often tungsten-based, white-light sources used in many characterizations setups like interferometer-based dispersion measurements, broadband attenuation characterization and numerous spectroscopy and microscopy setups [6] . The major disadvantage to all incandescent sources is the low brightness, which is determined by the filament temperature (black body radiation). Sources with higher output power utilize larger filaments with same brightness and the power that can be coupled to a single-mode fiber is therefore the same.

Moreover, the efficiency of light coupling from the filament to the fiber is generally low, resulting in only a small fraction of the light being available in the fiber. The super continuum source solves both the brightness and coupling issue and it is possible to create sources with the spectral width of a tungsten lamp and the intensity of a laser. The big issue in incandescent-light replacement sources based on super continuum generation is the pump source.

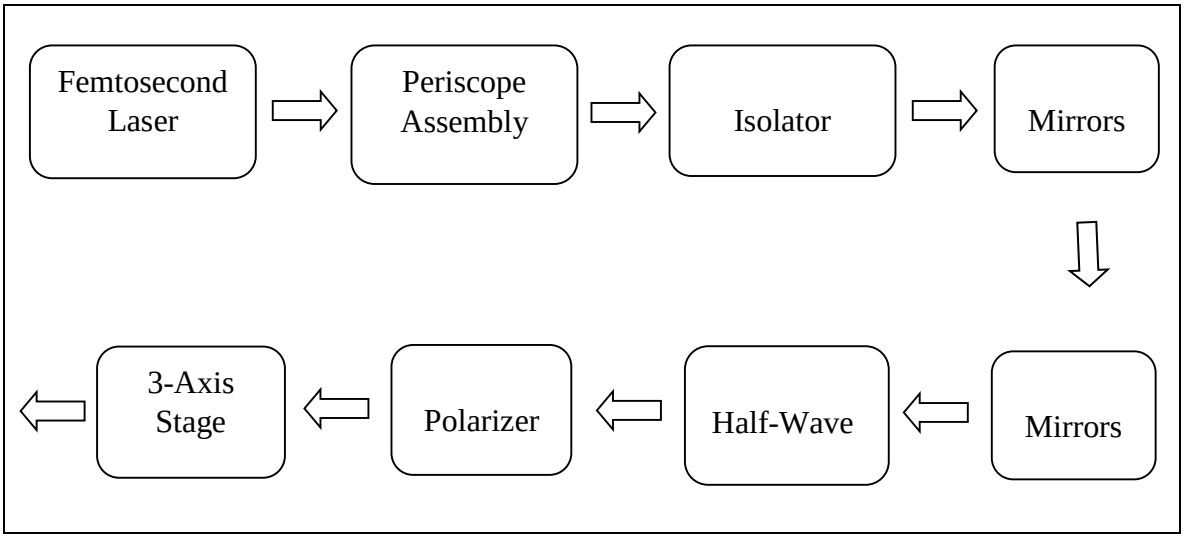

Fig. 1.2: Schematic diagram of Super continuum Generation Kit with non-linear Fiber cell.

A white-light source can be built very simply. In the extreme case, a super continuum source requires a large femtosecond laser system worth hundreds of thousands of dollars, and it is therefore crucial to develop more compact and cost-effective super continuum schemes. In this development, the long pulsed Nano and picosecond-sources around 1060 nm seem promising, especially the dual-wavelength pumping scheme shown that is expected to yield both cost-effective, compact and portable devices.

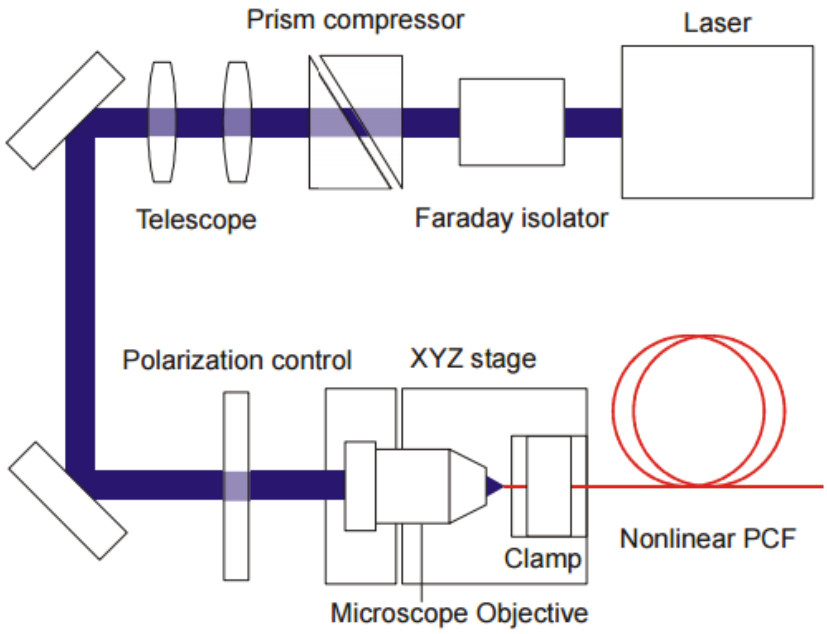

Fig. 1.3: Schematic drawing of a typical setup for super continuum generation using a Ti: Sapphire femtosecond laser and a short piece of highly nonlinear photonic crystal fiber [7].

Most SC experiments yield output in the mW-range, but systems with high average power have also been realized. As an example, a 900 nm broad SC source with an average output power of 2.4 W was recently demonstrated. The output was generated by pumping a 1 m long PCF with zero dispersion wavelength at 975 nm.

1.3.2 PCF Laser:

High powered PCF laser is one of the most important applications of PCF. Using duel-clad, step index fiber with a polymer outer cladding and a core doped with rare-earth ions, most commonly erbium [8]. The small core size required for single mode operation produces high power densities, which lead to detrimental non-linear effects. Different techniques have been developed to increase core size in step index laser fibers while still maintaining single mode output. Though these approaches have practical limitations in terms of thermal and mechanical stability, they're being used in some sophisticated cases.

A ring of air holes effectively confines the pump light to silica multimode pump core, known as inner cladding. A ring of air holes effectively confines the pump light to a silica multimode pump core. This type of PCF construction allows for a higher numerical aperture of the inner cladding than is possible using step index construction [9]. The higher NA permits efficient pumping with high power large-area-emitting pump diodes. The micro structured edges of

the inner cladding serve to scramble the pump modes, leading the efficient coupling of the pump power into active core.

Recently, photonic crystals have been developed in which the cores have also been co-doped with photorefractive materials, enabling fiber-Bragg gratings to be inscribed right into the core using UV laser light and further simplifying the architecture.

Air being the insulator, there had been a doubt that whether PCF would dissipate heat due to the large air gap in the cladding in high power lasers. But this doubt is cleared by now because it is found that there is no significant difference in heat dissipation for standard dual clad fiber lasers and properly designed dual clad PCF lasers.

Photonic crystal fiber is perhaps the most promising technology now-a-days to significantly lift the current power levels. This is because of its increased flexibility in single-mode core sizes, the increased numerical aperture of pump cores in double-clad fiber configurations and the high thermal stability of low-loss all glass fiber structures in laser research and technology.

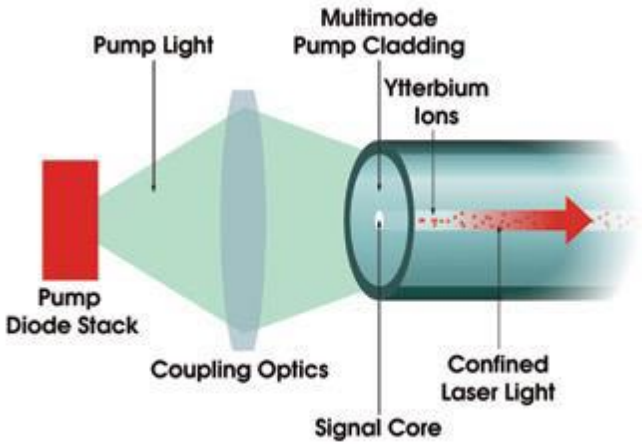

Fig. 1.4: A double-clad fiber laser converts low-beam-quality pump light into laser light with high beam quality [9].

1.3.3 Sensing Application:

PCF is vastly used in sensing application. Some sensing applications are given below.

Suspended Core Fiber:

Suspended Core Fiber (SCF) has been widely used in different sensing applications from physical science to life science due to its some discernible properties concerning sensing applications. Recently, advanced DNA sensing, broadband chemical sensing, and various sensing application has been exploited with SCF. The air holes of SCF are infiltrated with sample materials and core fields interact with these materials evanescently [11]. Large air

hole of SCF helps in speeding up the filling process by sample materials through the air holes in sensing applications. High air filling fraction ensures higher interaction between evanescent field and sample materials. Moreover, broad spectral features have made SCF unparalleled in sensing applications

In the above setup tapered SCF can be used to couple with the standard single mode fiber like SMF-28. Broad band optical source is needed for SCF based applications. Ultra low core of SCF enhances fiber nonlinearity which can be exploited in SC based sensor applications.

Increased sensitivity of fiber can be ensured by enhancing the evanescent field which demands more research work in SCF based fiber sensor.

Bragg grating Sensor:

In Bragg grating sensors in glass photonic crystal fibers we designed and fabricated a dedicated highly birefringent photonic crystal fiber (PCF). A Bragg grating inscribed in this PCF yields two Bragg reflection peaks and encodes pressure or transverse mechanical load in the spectral distance between those peaks [12]. The latter is practically insensitive to temperature and to longitudinal strain.

PCF Acoustic Sensor:

This is a compact sensor with fiber based microphone with no electrical parts. It is intended for underwater acoustic detection also known as hydrophone. The main property of such sensor is its high sensitivity at high acoustic frequencies. In such acoustic sensor, photonic crystal mirror and fiber-end mirror forms an FP Interferometer [13]. The reflected power changes with a change in the diaphram-fiber gap. The function of compact acoustic sensor is implemented at the end of a single-mode fiber.

Photonic-crystal mirror and fiber-end mirror forms a Fabry-Perot interferometer in acoustic sensors. The Photonic-crystal mirror provides a very thin, high reflectivity mirror, so that the Fabry-Perot is low order and has a high finesse.

Medical Application:

Optical coherence tomography (OCT) is a new technology for noninvasive cross-sectional imaging of tissue structure in biological system by directing a focused beam of light at the tissue to be image. The technique measures the optical pulse time delay and intensity of backscattered light using interferometry with broadband light sources or with frequency swept lasers. It is analogous to ultrasound imaging or radar, except that it uses light rather than sound or radio waves. In addition, unlike ultrasound, OCT does not require direct contact with the tissue being imaged. OCT depends on optical ranging; in other words, distances are measured by shining a beam of light onto the object, then recording the optical pulse time

delay of light. Since the velocity of light is so high, it is not possible to directly measure the optical pulse time delay of reflections; therefore, a technique known as low-coherence interferometry compares reflected light from the biological tissue to that reflected from a reference path of known length.

Different internal structures produce different time delays, and cross-sectional images of the structures can be generated by scanning the incident optical beam. Earlier OCT systems typically required many seconds or minutes to generate a single OCT image of tissue structure, raising the likelihood of suffering from motion artifacts and patient discomfort during imaging. To counter such problems, techniques have been developed for scanning the reference arm mirror at sufficiently high speeds to enable real-time.

1.4 THz Communication:

THz electromagnetic transmission (0.1-10 THz) has been an area of increasing interest and extensive research over the past few years. The border between far-IR and sub millimeter is still rather blurry and designation is likely to follow the methodology (bulk or modal-photon or wave), which is dominant in the particular instrument [14]. Despite great scientific interest at least the 1920s, the terahertz frequency range remains one of the least tapped regions of the electromagnetic spectrum. Sandwiched between traditional microwave and optical technologies where there is a limited atmospheric propagation path, little commercial emphasis has been placed on terahertz systems [15]. This has perhaps fortunately, preserved some unique science and applications for tomorrow's technology.

1.4.1 THz Communication Background:

- In 1960, THz is first used for image generation.
- In 1995, THz image was generated using Terahertz time-domain spectroscopy.
- At Rutherford Appleton laboratory in 2002, the European Space Agency (ESA) star Tiger Team produced first passive THz image of a hand.
- By 2004, Thru Vision Ltd, demonstrated the world's first compact THz camera for security screening application. This system successfully imaged guns and explosive under clothing.
- In mid-2007, scientists at the U.S. Department of Energy's Argonne National Laboratory, along with collaborators in Turkey and Japan, announced the creation of a compact device that can lead to portable, battery-operated sources of T-rays, or terahertz radiation. The group was led by Ulrich Welp of Argonne's Materials Science Division. This new T-ray source uses high-temperature superconducting crystals grown at the University of Tsukuba, Japan. These crystals comprise stacks of Josephson junctions that exhibit a unique electrical property: When an external voltage is applied, an

alternating current will flow back and forth across the junctions at a frequency proportional to the strength of the voltage; this phenomenon is known as the Josephson Effect. These alternating currents then produce electromagnetic fields whose frequency is tuned by the applied voltage. Even a small voltage – around two millivolts per junction can induce frequencies in the terahertz range, according to Welp.

- In 2008, engineers at Harvard University demonstrated that room temperature emission of several hundred nano watts of coherent terahertz radiation could be achieved with a semiconductor source. THz radiation was generated by nonlinear mixing of two modes in a mid-infrared quantum cascade laser. Until then, sources had required cryogenic cooling, greatly limiting their use in everyday applications.
- In 2009, it was shown that T-waves are produced when unpeeling adhesive tape. The observed spectrum of this terahertz radiation exhibits a peak at 2 THz and a broader peak at 18 THz. The radiation is not polarized. The mechanism of terahertz radiation is turbocharging of the adhesive tape and subsequent discharge.
- In 2011, Japanese electronic parts maker Rohm and a research team at Osaka University produced a chip capable of transmitting 1.5 Gbit/s using terahertz radiation.
- In 2013, researchers at Georgia Institute of Technology's Broadband Wireless Networking Laboratory and the Polytechnic University of Catalonia developed a method to create a graphene antenna: an antenna that would be shaped into graphene strips from 10 to 100 nanometers wide and one micrometer long. Such an antenna would broadcast in the terahertz frequency range.

1.5 THz Communication Application:

In recent years, THz communication have developed and successfully attracted the interest of scientist because of the various applications. Some important application of THz communication are given in this section.

1.5.1 Sensing

Terahertz sensing is enabling technology for detection of biological and chemical hazardous agents, cancer detection, detection of mines and explosives, providing security in buildings, airports, and other public space, short-range covert communications (in THz and sub-THz windows), and applications in radio astronomy and space research [16].

Most existing terahertz sources have low power and rely on optical means of the terahertz radiation. THz quantum cascade lasers using over thousand alternating layers of gallium arsenide and aluminum gallium arsenide have achieved high THz powers generated by optical means. Improved designs and using quantum dot medium for THz laser cavities are

expected to result in improved THz laser performance. Large THz powers are generated using free electron lasers or THz vacuum tubes.

High speed electronic devices (Schottky diodes, FETs and HBTs) have reached the THz range. A new approach called plasma wave electronics recently demonstrated terahertz emission and detection in GaAs-based and GaN-based HEMTs and in Si MOS, SOI, and FINFETs and in FET arrays, including the resonant THz detection.

1.5.2 Imaging

The terahertz band lies between the microwave and infrared regions of the electromagnetic spectrum. This radiation has very low photon energy and thus it does not pose any ionization hazard for biological tissues. It is strongly attenuated by water and very sensitive to water content. Unique absorption spectra due to intermolecular vibrations in this region have been found in different biological materials. These unique features make terahertz imaging very attractive for medical applications in order to provide complimentary information to existing imaging techniques [17]. There has been an increasing interest in terahertz imaging applications within the last few years and more and more terahertz spectra are being reported**.**

THz pulsed imaging actually can be viewed as an extension of the THz-TDS method. In addition to providing valuable spectral information, 2D images can be obtained with THz-TDS by spatial scanning of either the THz beam or the object itself. In this way, geometrical images of the sample can be produced to reveal its inner structures [18]. Thus, it is possible to obtain three-dimensional views of a layered structure.

When a THz pulse is incident on such a target, a train of pulses will be reflected back from the various interfaces. For each individual pulse in the detected signal, the amplitude and timing are different and can be measured precisely. The principle of time of flight technique is to estimate the depth information of the internal dielectric profiles of the target through the time that is required to travel over a certain distance. This permits looking into the inside of optically opaque material and it has been used for THz 3D imaging.

1.5.3 Spectroscopy

Terahertz (THz) spectroscopy holds large potential in the field of nondestructive, contact-free testing [19]. The ongoing advances in the development of THz systems, as well as the appearance of the first related commercial products, indicate that large-scale market introduction of THz systems is

THz spectroscopy is typically done with a single point measurement (with transmission geometry in most cases) of a homogenous sample and the resulting THz electric field can be

recorded as a function of time. Thus, it can be Fourier transformed to offer meaningful spectroscopic information due to the broadband nature of pulsed THz radiation. Although the spectral resolution is not as good as that with narrowband techniques, coherent detection of THz-TDS can provide both high sensitivity and time-resolved phase information [20]. This spectroscopic technique is primarily used to probe material properties and it is helpful to see where it lies in the electromagnetic spectrum in relation to atomic and molecular transitions.

THz spectroscopy is complementary to THz imaging and is primarily used to determine optical properties in the frequency domain. Since THz pulses are created and detected using short pulsed visible lasers with pulse widths varying from approximately 200 fs down to approximately 10 fs, it is now possible to make time resolved far-infrared studies with sub-picosecond temporal resolution. This was not achievable with conventional far-infrared studies. An important aspect of THz time-domain spectroscopy is that both the phase and amplitude of the spectral components of the pulse are determined. The amplitude and phase are directly related to the absorption coefficient and refractive index of a sample and thus the complex permittivity is obtained without requiring Kramers-Kronig analysis. Furthermore, another advantage of THz spectroscopy is that it is able to non-destructively detect differences because it uses radiation of sufficiently long wavelength and low energy that does not induce any phase changes or photochemical reactions to living organisms.

1.5.4 Information Showers

The inherently small communication range of THz cells inspired the community to search for the scenarios, where small (few meters radius maximum) and extremely high-rate (up to Tbps) cells can be used in the most efficient way. This group of ideas is typically branded as "information shower" or, less frequently, "data shower".

The concept suggests deployment of THz access points (APs) in the areas with high human flow (e.g. gates to the metro station, public building entrances, shopping mall halls, etc.). With such a deployment strategy, each of the passing user is able to receive bulk data (up to several GBs), just while passing this AP. Such information showers can be used do seamlessly deliver software updates as well as other types of heavy traffic, such as high-quality video (e.g. a movie to watch in a train). As the contact time between the user's terminal is very small (in the order of seconds), the introduction of information showers to the existing networking architecture requires partial redesign of several layers to enable fast nodes association and authentication as well as timely content delivery to the appropriate information shower and caching it there. Meanwhile, it has been recently demonstrated that in certain scenarios introduction of just few THz APs and forwarding all the heavy and delay-tolerant traffic to them whenever possible, allows to substantially offload the macro-scale network (e.g.WLAN or cellular) [20].

1.5.5 Mobile Access:

The applicability of THz communications to typical usage scenarios (e.g. indoor WLAN access) is limited due to considerable propagation losses. This could be addressed by trading the capacity of THz access points for coverage, primarily by reducing the utilized bandwidth and moving the entire communications from above 1 THz to the so-called "lower terahertz" carriers around 300GHz. As a result, it is possible to create reliable wireless links over tens of meters while retaining the capacity of tens of gigabits per second, which makes Wi-Fi-like THz access points (or even femto-cells for cellular access) become feasible. This application is both one of the most desirable ones, but also very challenging due to requirement of reliable beam tracking and effective medium access control. Section IV studies some of the engineering tradeoffs to enable this use case.

1.5.6 Security-Sensitive Communications:

An ability to create highly directional beams with miniature size antenna arrays in conjunction with the high theoretical capacity of THz links results in a number of benefits for the security-sensitive usage, especially in military applications. The typical military scenario presents a battlefield with numerous heterogeneous units (soldiers, armored personnel carriers, tanks, etc.) forming a THz ad hoc network. The primary advantage of the considered technology in comparison to lower frequencies is a physical inability to eavesdrop or even notice the transmission for any node located outside the transmitter beam. Therefore, the security of the transmitted data can be ensured not only by the proper encryption scheme, but also by the geometry of the network itself. The idea of utilizing directional THz antennas to improve the security of the military links has been recently expanded for the civil use as well. Particular use cases range from the ATM with wireless authentication up to the kiosk downloading. The nature of THz links with limited communication range and narrow beams also provides fruitful ground for the physical layer security techniques, which, generally speaking, introduce some artificial "noise "into the signal before the transmission. The confidentiality of the message in this case is ensured by the fact that only the valid received, transmitter is now pointing to, has sufficiently good channel to decode the data.

1.5.7 Fiber Equivalent Wireless Links:

The strategy for next generation wireless networks (5G and Beyond) envision the appearance of numerous high-rate small cells, operating in the mm Waves spectrum [21]. This approach is considered as almost the only feasible solution to rapidly increase the area spectral efficiency, and thus, support emerging bandwidth greed applications in the area of virtual and augmented reality, holographic communications and many more. In addition to a number of challenges with interference minimization, handover support, there is also a challenge to

provide a reliable front haul and backhaul links, where a wired or optical solutions not all the time the best option. For instance, the recent proposals by Huawei and many others suggest deployment of high-rate small cells on street lamps, where the constant power supply is presented by design, while the data link is not. In such a case, wireless front haul/backhaul is considered as a promising alternative. Moreover, the recent suggestions of applying UAVs. For coverage and capacity extensions cause the need to provide the wireless connectivity for them as well. The envisioned data rates in mm Wave small cells (access link) are in the order of several gigabits-per-second, thus, the capacity of the front haul/backhaul link should be several times higher to guarantee reliable and timely data delivery from multiple users, currently connected to the small cell. With this in mind, the bandwidth available in the THz frequencies is an attractive resource, while the high propagation loss in THz band (backhaul links might be considerably longer than the front haul ones) can be compensated by the extremely high antennas directivity. The feasibility of multi-gigabit-per second wireless links in the lower THz band for the distances up to 1 km long has been recently experimentally validated in [22] and [23].

1.5.8 Connectivity with Miniature Devices:

The possibility to create micro-scale transceivers operating in the THz band naturally leads to the desire of incorporating the envisioned micro- and nano-scale robots with such a feature. These so called "nanorobots" usually incorporate a very primitive logic due to size and power consumption limitations and, thus, are technically incapable to perform any substantial task alone. On the contrary, by connecting with numerous other nanorobots that can form a network, capable to assist the society in many different areas, starting from the environmental sensing and medicine and up to PPDR. In contradiction to large-scale THz communication systems, envisioned to be built around massive antenna arrays of hundreds or even thousands of elements [24], micro- and nano- ones are to be equipped with very basic radio modules with just a few (or even a single) antennas. Consequently, the communication range in these nano networks is limited to centimeters. At the same time, the capacity of the links is several orders of magnitude higher that the envisioned data rate, thus, living the room for trivial and non-efficient modulations and coding schemes, such as On/Off Keying [25].

1.5.9 On-Chip and Chip-to-Chip Links:

Due to several limitations of further increase in the CPU frequency, the horizontal scaling of the computing power by incorporation of more and more computing cores per chip is today considered as the primarily approach. Unfortunately, majority of the typical computer tasks do not feature so-called "data parallelism", so the cores have to constantly interact with each other sharing the common data and synchronizing their activities. Moreover, this communications have to be extremely fast and reliable. Therefore, providing an underlying

connectivity solution for the chips/cores/registers/caches/etc. is of crucial importance for the desired computational performance level. Naturally, with the growth in the amount of communication nodes, computer scientists start more and more often reusing the solutions from the communications and networking world, where many problems they face today (e.g. time synchronization, channel access, routing, etc.) have already been addressed. This trend is mostly covered by the umbrella of ”Networks-on-Chips” and, simplifying a lot, suggests reusing some of the networking techniques to design efficient solutions for data exchange between different entities within a single computer. There is also a room for the wireless solutions in this world, since in case of a substantial number of cores per chip (e.g. 64 and more) the wired network concepts face a number of issues with topology complexity and routing. While the community aims to utilize the microwave and mm Waves spectrum for board-to-board communications [26], on-chip and chip to- chip links can only be enabled with a substantially smaller transceivers (sub-mm scale), thus, calling for the need of THz band radio to be used. Graphene-based THz electronics is one of the primarily enablers of massive multicore wireless networks-on-chip [27].

1.5.10 Safety Monitoring and Quality Control:

THz radiation can also be used for detecting pollutants, biological and chemical detection, and therefore can be used to monitor the process of food preservation and food processing. The characteristics of THz wave, penetrating objects and security, can be used for non-contact, no injury to detect specific substances, such as hidden explosives, drugs, weapons. As a result of the strong capacity of penetration and low energy of THz electromagnetic waves (completely harmless to humans), THz imaging can completely replace the X-ray examination, CT scan, and be used in the material nondestructive monitoring and vital security sector and chemical and biological weapons inspection.

Fig. 1.5: Safety Monitoring [28]

1.6 Motivation for the Thesis:

Currently, more interest has been focused for terahertz (THz) spectrum ranging from 0.1 to 10 THz as this band of frequency has so many promising and potential applications as medical diagnostics, imaging, security, sensing and many more. The wide spread applications opportunity of THz technology motivated the optoelectronics community to make concentrated effort in the development of better THz sources and detectors. As a consequence, the last decade has been flavored commercial availability of THz sources and detectors. Simultaneously, available waveguides are not enough to effective transmitting THz waves. Although dry air exhibits lowest absorption in this band, free space propagation of THz is not enough beneficial due to unwanted loss introduced during coupling, transporting and managing THz beam [29]. Therefore, the main challenge faced by the researchers is to design a waveguide structure that confine high power fraction in the dry air and confine low power fraction within material thus results low loss wave guiding. Since there are a lot of advantages of guided propagation waves, research is being carried out both theoretically and practically using dielectric metal-coated tubes, Bragg fibers, hollow core fibers, Flexible tube lattice fibers . Very recently, research trend using THz frequency has been turning toward porous-core PCFs owing to its low EML and high mode power confinement in the air.

The new research field, new scope, always expanding application of THz range, have motivated us to research further on THz range photonic crystal fiber (PCF).

1.7 Objectives of the Thesis

The thesis concentrates on developing a THz PCF model of low confinement loss and highly birefringent, very low EML and flattened Dispersion. To pursue our goal we have investigated different models and their characteristics. Finally we have come to a conclusion about which model would serve our purpose best.

The objectives of this thesis are

i. To design a THz PCF, which will have high birefringent and flattened dispersion.
ii. To design another THz PCF, which will have very low loss.

The outcome of this thesis is the development of two different model of PCF which can be effectively used in many important applications.

1.8 Organization of the Thesis

The thesis consists of five chapters.

Chapter -1: Consist of introduction and application of Photonic Crystal Fiber (PCF), the historical background of THz communication and its application, Motivation for thesis and the objectives of the thesis.

Chapter -2: Consists of Mathematical Discussions and analysis with parameters and Equations. Mathematics, Governing Physics & Computational analysis are described briefly. It provides the finite element method (FEM), boundary conditions and discussion regarding them and summaries mathematical equation and solutions.

Chapter -3: Consists of the properties of photonic crystal fiber like dispersion, polarization, birefringence, Confinement loss, Effective material loss (EML).

Chapter -4: Consists of the design of proposed models and Electric field distribution.

Chapter -5: Consists of various analysis and the results.

Chapter -6: It is the concluding chapter. It contains the summary of the work. The chapter also highlights scopes for future work. All references are placed at the end of this thesis.

Chapter 2

Governing Physics

Photonic crystal fibers (PCFs) which are characterized by a cladding of air capillaries most commonly arranged in a triangular lattice, have been a key topic of research in the field of optical fiber communication. The form of the central defect core is responsible for the PCF's light guiding mechanism: index guiding in the case of a solid core, or band gap guiding when low-index or hollow cores are used. Numerical software plays an important role in the design of waveguides and fibers. For a fiber cross section, even the simplest shape is difficult and cumbersome to deal with analytically. As this thesis is concentrated on index guiding PCF, the methodology of simulating the different characteristics of PCF will be discussed here.

2.1 Governing Physics:

At any frequency ω, optical fibers can support a finite number of guided modes whose spatial distribution is a solution of the wave equation-

$$\nabla \times (n^{-2} \times \vec{H}) - k_0 \vec{H} = 0 \tag{2.1}$$

Called the Hemholtz equation. While the solutions support all the appropriate boundary conditions, the fiber can also support a continuum of unguided radiative modes. In the Hemholtz equation, the optical mode analysis is made on a cross-section in the x-y plane of the fiber. The quantity $\vec{H}$ represents the magnetic field and has the form

$$\vec{H}(x, y, z) = \vec{H}(x, y)e^{-j(\omega t - \beta z)} = 0 \tag{2.2}$$

Where β is the propagation constant. Equation (2.2) is solved for eigenvalues of the effective index λ= jβ. The equation (2.2) is defined for longitudinally-invariant structures composed of nonmagnetic anisotropic materials with diagonal permittivity tensors and $e^{j\omega t}$ time dependence of the field; it is possible to get a vectorial wave equation expressed only in terms of the transverse components of the magnetic field as follows:

$$\begin{bmatrix} \frac{\partial}{\partial y}[\frac{1}{n_{zz}^2}(\frac{\partial H_Y}{\partial x} - \frac{\partial H_Z}{\partial y})] \\ -\frac{\partial}{\partial x}[\frac{1}{n_{zz}^2}(\frac{\partial H_y}{\partial x} - \frac{\partial H_x}{\partial y})] \end{bmatrix} - \begin{bmatrix} \frac{1}{n_{yy}^2}\frac{\partial}{\partial x}(\frac{\partial H_x}{\partial x} + \frac{\partial Hy}{\partial y}) \\ \frac{1}{n_{xx}^2}\frac{\partial}{\partial y}(\frac{\partial H_x}{\partial x} + \frac{\partial H_y}{\partial y}) \end{bmatrix} + k_0^2 n_{eff}^2 \begin{bmatrix} \frac{1}{n_{yy}^2}H_x \\ \frac{1}{n_{xx}^2}H_y \end{bmatrix}$$

$$= \boldsymbol{k}_0^2 \begin{bmatrix} \boldsymbol{H}_x \\ \boldsymbol{H}_y \end{bmatrix} \tag{2.3}$$

In equation (2.3), k_0 is the free space wave number, n_{eff} is the mode index, n_{xx}, n_{yy}, n_{zz} are the diagonal entries of the relative permittivity tensor, associated with the x, y, z components of the electric field.

2.2 Finite Element Method

The finite element method (FEM) is a numerical technique for finding approximate solutions to boundary value problems for partial differential equation. It uses subdivision of a whole problem domain into simpler parts, called finite elements, and variational methods from the calculus of variation to solve the problem by minimizing an associated error function. Analogous to the idea that connecting many tiny straight lines can approximate a larger circle, FEM encompasses methods for connecting many simple element equations over many small subdomains, named finite elements, to approximate a more complex equation over a larger domain.

While solving the eigenvalue equation, COMSOL Multiphysics uses the finite element method. It sub-divides the object into very small but finite size elements. This process is called 'meshing' and is shown in the following figure for the solid-core PCF.

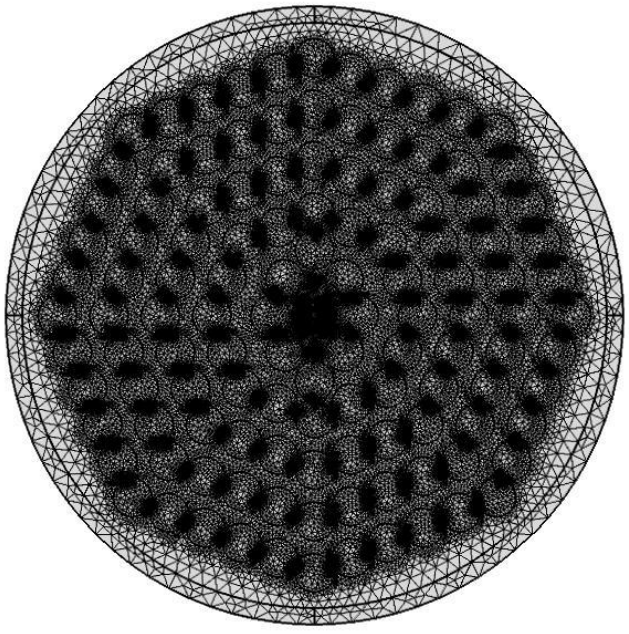

Fig. 2.1: Solid-core PCF with meshing

Each element of the mesh is governed by a set of characteristic equations which describe its physical properties and boundary conditions. These equations are then solved as a set of simultaneous equations to compute the effective index of the modes supported by the fiber. To obtain the nodal field values, the usual Rayleigh-Ritz procedure is employed for the

stationary solution of the functions with respect to each of the nodal variables. This can be written in a matrix eigenvalue equation:

$$[A]\{x\} - [B]\{x\} = 0 \tag{2.4}$$

Where [A] and [B] are real symmetric matrices, & [B] is also positive definite. The eigenvalue λ may be k_0^2 or β^2 depending on the variational formulation and {x} is the eigenvectors representing the unknown nodal field values. It is most desirable for the resulting matrix equation to be of this canonical form, to allow for an efficient and robust solution. This equation (2.4) can be solved by one of various standard subroutines to obtain different eigenvectors and eigenvalues.

There are various types of elements such as one, two and three dimensional elements available for use in finite element formulations. When the configuration and other details of the problem can be described in terms of two independent spatial coordinates, the two dimensional elements can be used. Each element is essentially a simple unit within which the unknown can be described in a simple manner. The basic and the simplest element useful for two-dimensional analysis is the triangular element. The smaller the size of the element, the more accurate is the final solution.

By dividing the waveguide cross section into triangular elements, the unknown H is also considered as to be discretized into corresponding sub-regions. These elements are easier to analyze rather than analyzing the distribution over the whole cross section.

2.3 Applications of FEM:

Discretizing the computational domain into triangular elements lead to the following discretized weak formulation:

$$\sum_{\substack{boundary\\elements}} \left\{ -\int_{\tau_e} \frac{1}{n_{zz}^2} w_y \left(\partial x H_y - \partial y H_x\right) dy - \int_{\tau_e} \frac{1}{n_{zz}^2} w_x \left(\partial x H_y - \partial y H_x\right) dx \right.$$

$$\left. -\int_{\tau_e} \frac{1}{n_{yy}^2} w_x \left(\partial x H_x + \partial y H_y\right) dy + \int_{\tau_e} \frac{1}{n_{xx}^2} w_y \left(\partial x H_x + \partial y H_y\right) \right\} dx$$

$$+ \sum_{\substack{\text{int}erface\\elements}} \left\{ -\int_{\tau_{\text{int},e}} \frac{1}{n_{yy}^2} w_x \left(\partial x H_x + \partial y H_y\right) dy + \int_{\tau_{\text{int},e}} \frac{1}{n_{xx}^2} w_y \left(\partial x H_x + \partial y H_y\right) dx \right\}$$

$$+ \sum_{\substack{triangular\\elements}} \iint_{\Omega_e} \left\{ \frac{1}{n_{zz}^2} w_y \left(\partial x w_y - \partial y w_x\right)\left(\partial x H_y - \partial y H_x\right) \right.$$

$$+\left[\partial x\left(\frac{1}{n_{yy}^2}w_x\right)+\partial y\left(\frac{1}{n_{xx}^2}w_y\right)\right]\left(\partial xH_x+\partial yH_y\right)$$

$$+k_0^2 n_{eff}^2\left(\frac{1}{n_{yy}^2}w_xH_x+\frac{1}{n_{xx}^2}w_yH_y\right)-k_0^2\left(w_xH_x+w_yH_y\right)\Big\}dxdy$$

$$=\mathbf{O} \tag{2.5}$$

Here, w_x & w_y denotes weight functions, Ω_e is he area of each triangular element, $\tau_{int,}$ is the line element at the interface between different materials and τ_e is the line element at the computation boundaries. Approximating the fields using quadratic nodal-based basis functions will lead to a sparse generalized matrix eigenvalue equation, which can be solved using an eigenvalue solver to obtain the eigenvalues related to the modal indices (n_{eff}) and eigenvectors associated with the transverse components of the magnetic field $[Hx \;\; Hy]^T$ of the corresponding nodes.

2.4 Boundary and Interface Conditions

The boundary conditions specify the value of electric & magnetic fields or their derivatives or the products with some directional vectors on the boundary of the computation domain to find a particular solution. Three types of boundary conditions are primarily needed to be considered during the numerical computation. These are- 1) Perfect Electric Conductor 2) Perfect Magnetic Conductor 3) Perfectly Matched Layer.

The interior boundaries of the cross-sectional geometry of the PCF are set at continuity boundary conditions. The outermost boundary of the cross-section is set at perfect electric conductor boundary condition when solving for magnetic field intensity, H. Perfect magnetic conductor boundary condition is used when solving for electric field, E. This is a valid boundary condition as the radius of the geometry is chosen large enough for the electric or magnetic field to decay to zero.

2.4.1 Perfect Electric Conductor:

This boundary condition can be expressed as,

$$n\cdot\vec{B}=\mathbf{O} \tag{2.6}$$

$$n\times\vec{E}=\mathbf{O} \tag{2.7}$$

Equation (2.7) sets the tangential component of the electric field to zero at the boundary

Here, $\hat{n}$ is the unit normal vector to the boundary. According to this condition, tangential components of $\vec{E}$ and normal components of $\vec{B}$ is continuous across any interface.

2.4.2 Perfect Magnetic Conductor:

In this case, the boundary condition is expressed as-

$$\boldsymbol{n} \cdot \overrightarrow{\boldsymbol{D}} = \mathbf{0} \tag{2.8}$$

$$\boldsymbol{n} \times \overrightarrow{\boldsymbol{H}} = \mathbf{0} \tag{2.9}$$

Equatio (9) sets the tangential component of the magnetic field to zero at the boundary

In this case, the tangential components of $\vec{H}$ and normal components of $\vec{D}$ is continuous across any interface.

2.4.3 Continuity:

The continuity boundary condition,

$$\overline{n} \times (\overline{H_1} - \overline{H_2}) = 0 \tag{2.10}$$

$$\overline{n} \times (\overline{E_1} - \overline{E_2}) = 0 \tag{2.11}$$

is the natural boundary condition ensuring continuity of the tangential components of the electric and magnetic fields.

2.4.4 Perfectly Matched Layer:

Numerical simulation of propagating waves in unbounded spatial domains is a challenge common to many branches of engineering and applied mathematics. Perfectly matched layers (PML) are a novel technique for simulating the absorption of waves in open domains. The equations modeling the dynamics of phenomena of interest are usually posed as differential equations or integral equations which must be solved at every time instant. In many application areas like general relativity and acoustics, the underlying equations are systems of second order hyperbolic partial differential equations. In numerical treatment of such problems, the equations are often rewritten as first order systems and are solved in this form. For this reason, many existing PML models have been developed.

A perfectly matched layer is an artificial boundary condition implying perfect absorption of incident field. This boundary condition is required for approximating infinite zone beyond the waveguide outer edge to a finite domain of numerical analysis. Effect of PML on

numerical solutions obtained will be more prominent when confinement of field in the PCF is weak. This layer can also be utilized to find out the complex part of effective index.

There are several different PML formulations. However, all PML's essentially act as a lossy material. The lossy material, or lossy layer, is used to absorb the fields traveling away from the interior of the grid. The PML is anisotropic and constructed in such a way that there is no loss in the direction tangential to the interface between the lossless region and the PML. However, in the PML there is always loss in the direction normal to the interface.

The PML was originally proposed by J. P. Berenger in 1994[30]. In that original work he split each field component into two separate parts. The actual field components were the sum of these two parts but by splitting the field Berenger could create an (non-physical) anisotropic medium with the necessary phase velocity and conductivity to eliminate reflections at an interface between a PML and non-PML region.

The PML region can be viewed as a perfect absorber with a certain magnitude of conductivity. However, the optimized conductivity is calculated from certain sets of equations. In our work, we have considered cylindrical PML available in the commercial software.

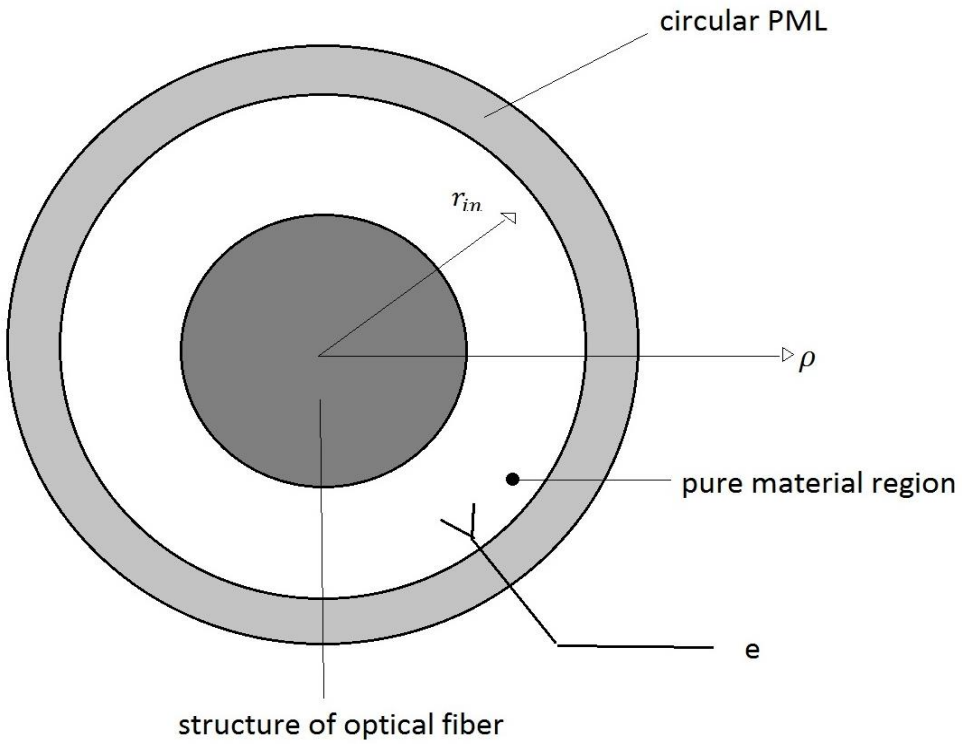

Fig. 2.2 PML region surrounding the waveguide structure.

Here, e is the thickness of the PML layer which is ideally a multiple of the operating wavelength.

The wave equations in the PML can be done after doing rigorous analysis-

$$\Delta \times H = j\omega n^2 sE \tag{2.12}$$

$$\Delta \times E = -j\omega \mu_0 sH \tag{2.13}$$

$$s = 1 - j\frac{\sigma_e}{\omega n^2 \in_0} = 1 - j\frac{\sigma_m}{\omega \mu_0} \tag{2.14}$$

Here,

E: Electric field

H: Magnetic Field

σ_e: Electric conductivity of PML

σ_m: Magnetic conductivity of PML

To avoid numerical reflection, conductivity in the PML region is graded to a peak value rather than an abrupt rise as shown in Fig. 2.5.

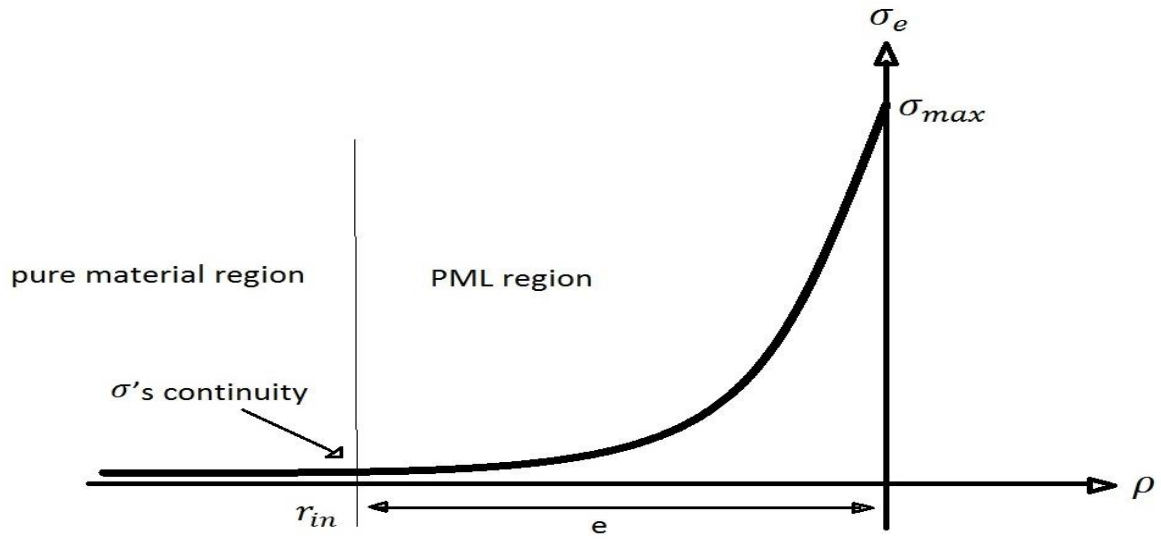

Fig. 2.3: Grading of PML conductivity

In this case, the PML parameters become-

$$s = 1 - jk\left(\frac{\rho - r_{in}}{e}\right)^2 \quad \text{in PML region}$$

$$= 1 \quad \text{in other regions} \tag{2.15}$$

Where k is defined for wavelength by

$$k = \frac{3\lambda}{4\pi n_e} \ln\left(\frac{1}{R}\right) \tag{2.16}$$

Where R is the reflection coefficient of electromagnetic field from the interface to be minimized.

$$R = \exp[(-2\frac{\sigma_{\max}}{n \in_0 n_0}\int_0^d (\frac{\rho}{d})^m)dp] \tag{2.17}$$

For a perfectly matched condition to secure zero reflection from the interface, we can write-

$$\frac{\sigma_e}{n^2 \in_0} = \frac{\sigma_m}{\mu_m} \tag{2.18}$$

For this maximum conductivity is defined as below,

$$\sigma_{\max} = \frac{m+1 \in_0 cn}{2d} \ln(\frac{1}{R}) \tag{2.19}$$

Here, m is the order of polynomial for grading conductivity. These equations imply that, minimum reflection will occur for a maximum conductivity. However, numerical error terms imply that there is an optimum magnitude of reflection for accurate propagation constant. A stable value of complex effective index can be obtained by altering the thickness of PML and distance of PML from center of the PCF.

Chapter 03

Some Properties of Optical Fiber

The introduction of optical fiber system revolutionized the communication network. The low transmission loss and the large bandwidth capability of the fiber systems allow signals to be transmitted for establishing communication contacts over large distances with few or no provisions of intermediate application. There are many properties of optical fiber such as dispersion, birefringence, effective material loss, confinement loss, bending loss, non-linearity etc. The most focused properties of fiber are described below:

3.1 Dispersion in an Optical Fiber:

In optics, dispersion is the phenomenon in which the phase velocity of a wave rest on its frequency, or otherwise when the group velocity depends on the frequency. Dispersion is most often defined for light waves, but it may occur for some kind of wave that interacts with a medium or passes through an inhomogeneous geometry (e.g. a waveguide), such as sound waves.

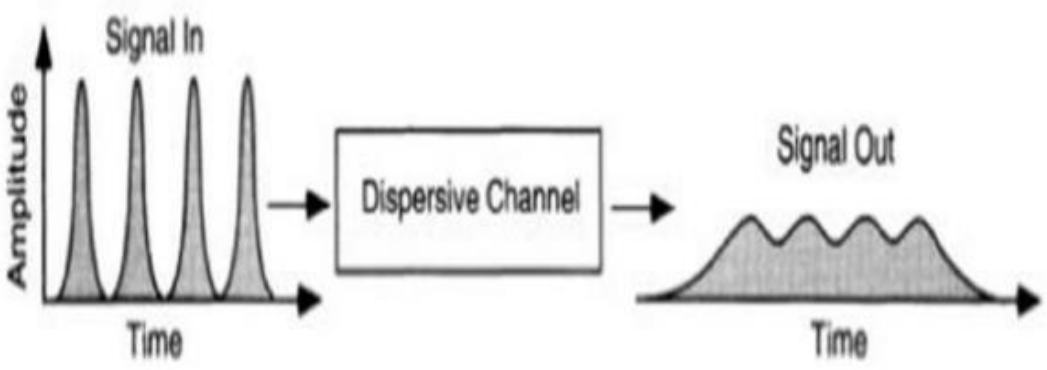

Fig. 3.1: Pulse Degradation from Dispersion in Photonic Crystal Fiber

Intermodal dispersion in multimode fibers leads to considerable broadening of short optical pulses (~10ns/km). In the geometrical-optics description, such broadening was attributed to different paths followed by different rays. In the modal description it is related to the different mode indices (or group velocities) associated with different modes. The main advantage of single-mode fibers is that intermodal dispersion is absent simply because the energy of the injected pulse is transported by a single mode. However, pulse broadening does not disappear altogether. The group velocity associated with the fundamental mode is frequency dependent because of chromatic dispersion. As a result, different spectral components of the pulse travel at slightly different group velocities, a phenomenon referred to as group-velocity dispersion (GVD), intra-modal dispersion, or simply fiber dispersion. Intra-modal dispersion has two

contributions, material dispersion and waveguide dispersion. We consider both of them and discuss how GVD limits the performance of light-wave systems employing single-mode fibers.

3.1.1 Group Velocity Dispersion:

The group velocity of a propagating wave is a measure of the wavelength dependence of the effective index in any waveguide. Mathematically [31].

$$v_g = \left(\frac{d\beta}{d\omega} \right)^{-1} \tag{3.1}$$

In an optical fiber of length L, a spectral component of frequency ω would arrive at the output end of the fiber after a time delay $T=\left(\frac{L}{v_g}\right)$. The frequency dependence of the group velocity leads to pulse broadening simply because different spectral components of the pulse disperse during propagation and do not arrive simultaneously at the fiber output. If $\Delta\omega$ is the spectral width of the pulse, the extent of pulse broadening for a fiber of length L is governed by-

$$\Delta T = \left(\frac{dT}{d\omega} \right) \Delta\omega = \frac{d}{d\omega} \frac{L}{v_g} \Delta\omega = L \left(\frac{d^2\beta}{d\omega^2} \right) \Delta\omega = L\beta^2 \Delta\omega \tag{3.2}$$

Where β_2 corresponds to second order dispersion, known as the GVD parameter. The dispersion length for an optical pulse of input pulse width T_0 is given by [32]-

$$L_D = \frac{T_0}{|\beta_2|} \tag{3.3}$$

The dispersion parameter D can vary considerably when the operating wavelength is shifted from 1.3μm. The wavelength dependence of D is governed by the frequency dependence of the mode index. The equation of D can be written as,

$$D = \frac{2\pi c}{\lambda^2} \frac{d}{d\omega} \left(\frac{L}{v_g} \right) = -\frac{2\pi}{\lambda^2} \left(\frac{dn}{d\omega} + \omega \frac{d^2 n}{d\omega^2} \right) \tag{3.4}$$

D can be broken in terms of waveguide dispersion & material dispersion as [33] -

$$D(\lambda) = D_w(\lambda) + D_m(\lambda) \tag{3.5}$$

3.1.2 Material Dispersion:

Material dispersion occurs because the refractive index of silica, the material used for fiber fabrication, changes with the optical frequency component. On a fundamental level, the origin of material dispersion is related to the characteristic resonance frequencies at which the material absorbs the electromagnetic radiation. Far from the medium resonances, the refractive index n (λ) is well approximated by the Sellmeier equation [34]-

$$n^2(\lambda) = 1 + \frac{\beta_{1\lambda^2}}{\lambda^2 - c_1} + \frac{\beta_{2\lambda^2}}{\lambda^2 - c_2} + \frac{\beta_{3\lambda^2}}{\lambda^2 - c_3} \tag{3.6}$$

3.1.3 Waveguide Dispersion:

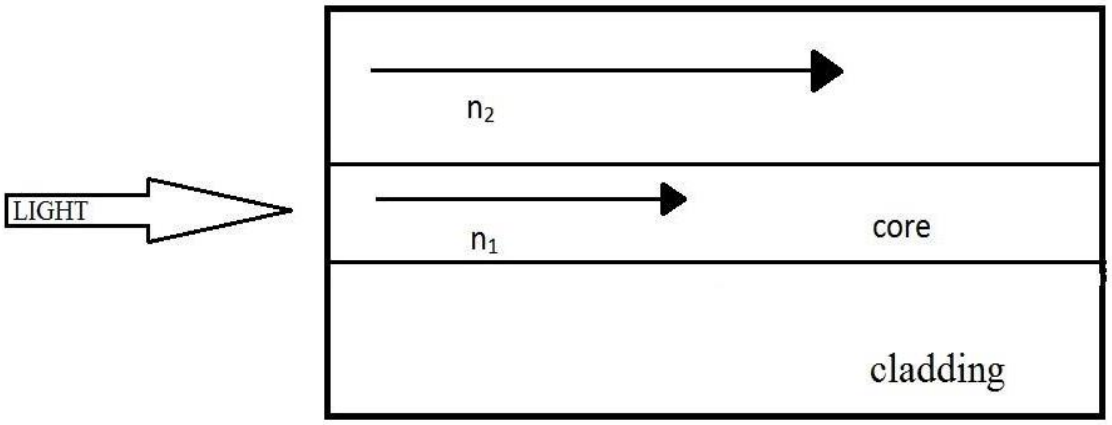

Fig. 3.2: Waveguide Dispersion in optical fiber.

The origin of waveguide dispersion can be understood by considering that a guided wave has a frequency-dependent distribution of wave vectors (k vectors), whereas a plain wave (as the reference case) has only a single wave vector, which points exactly in the propagation direction. The waveguide dispersion parameter Dw depends on the V parameter of the fiber & is given by [35]

$$D_w = -\frac{2\pi\Delta}{\lambda^2}\left[\frac{n_g^2}{n_2\omega}\frac{Vd^2(Vb)}{dV^2} + \frac{dn_{2g}}{d\omega}\frac{d(Vb)}{dV}\right] \tag{3.7}$$

Where, V parameter & the normalized propagation constant b are defined as [36]

$$V = \frac{2\pi\Delta}{\lambda^2}(n_{core}^2 - n_{eff}^2) \tag{3.8}$$

$$b = \frac{\frac{\beta}{k_0} - n_2}{n_1 - n_2} \tag{3.9}$$

The main effect of waveguide dispersion is to shift λ_{ZD} by an amount 30-40 nm so that the total dispersion is zero near 1.31 μm. It also reduces D from its material value (λ) in the wavelength range 1.3-1.6μm that is of interest for optical communication systems. Typical values of D is in the range of 15 to 18 ps/(km-nm) near 1.55 μm[37].This wavelength region is of considerable interest for light wave systems because fiber losses become minimum near 1.55 μm[38, 39,40]. High values of D limit the performance of 1.55 μm light wave systems.

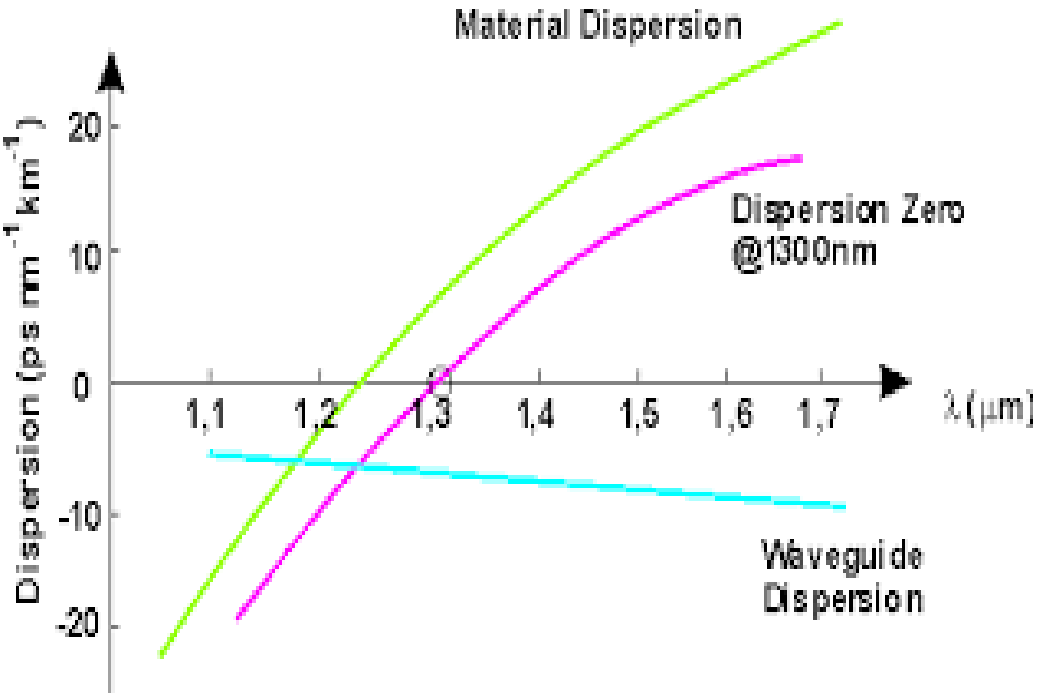

Fig. 3.3: Relative contributions of material dispersion D_m(λ) and waveguide dispersion D_w (λ) for a conventional single-mode fiber [34] .

Since the waveguide contribution D_w (λ) depends on fiber parameters such as the core radius 'a' and the index difference 'A', it is possible to design the fiber such that λ_{ZD} is shifted into the vicinity of 1.55 μm. Such fibers are called dispersion shifted fibers. It is also possible to tailor the waveguide contribution such that the total dispersion D is relatively small over a wide wavelength range extending from 1.3 to 1.6μm. Such fibers are called dispersion flattened fibers. The design of dispersion modified fibers involves the use of multiple cladding layers and a tailoring of the refractive-index profile. Waveguide dispersion can also

be used to produce dispersion-decreasing fibers in which GVD decreases along the fiber length because of axial variations in the core radius. In another kind of fibers, known as the dispersion-compensating fibers, GVD is made normal and has a relatively large magnitude.

3.1.4 Polarization Mode Dispersion

It can limit the performance of single-mode systems, occurs because although the single-mode fiber can sustain only one transverse mode, it can carry this mode with two different polarizations, and slight imperfections or distortions in a fiber can alter the propagation velocities for the two polarizations. Dispersion limits the bandwidth of the fiber because the spreading optical pulse limits the rate that pulses can follow one another on the fiber and still be distinguishable at the receiver.

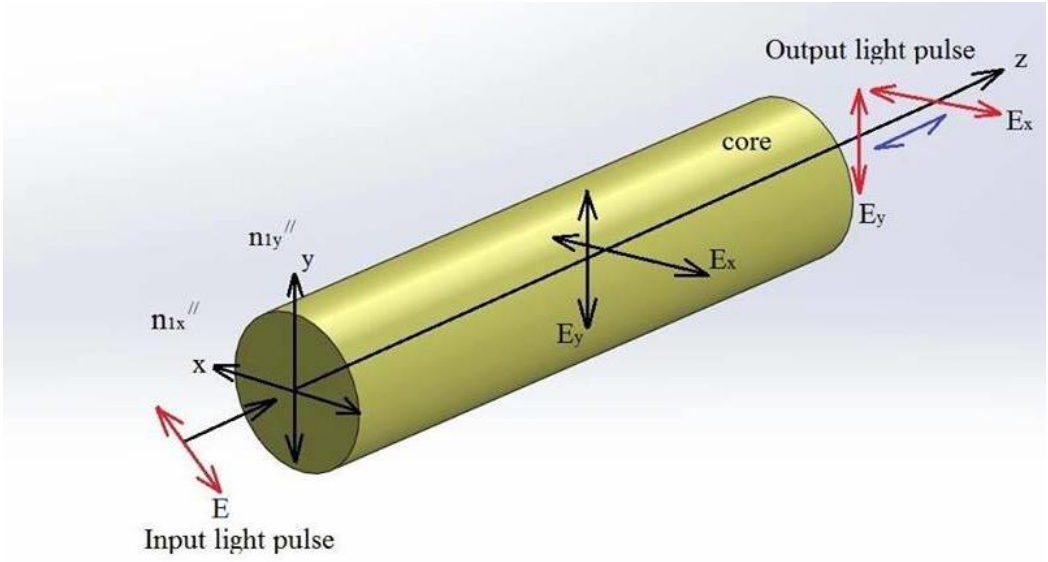

Fig. 3.4: Polarization mode dispersion of optical fiber.

3.2 Polarization & Birefringence of light in Optical Fiber:

Birefringence is the optical property of a material having a refractive index that depends on the polarization and propagation direction of light. These optically anisotropic materials are said to be birefringent. The birefringence is often quantified as the maximum difference between refractive indices exhibited by the material. Crystals with non-cubic crystal structures are often birefringent, as are plastics under mechanical stress. The degree of modal

birefringence B_f of the PM-PCF (Polarization Maintaining PCF) is a measure of the separation of the two cross polarization modes in the fiber & is defined by [41] -

$$B = \left| n_y - n_x \right| \tag{3.10}$$

Where,

B=Birefringence of fiber

n_y,n_x=Refractive index of two polarization modes

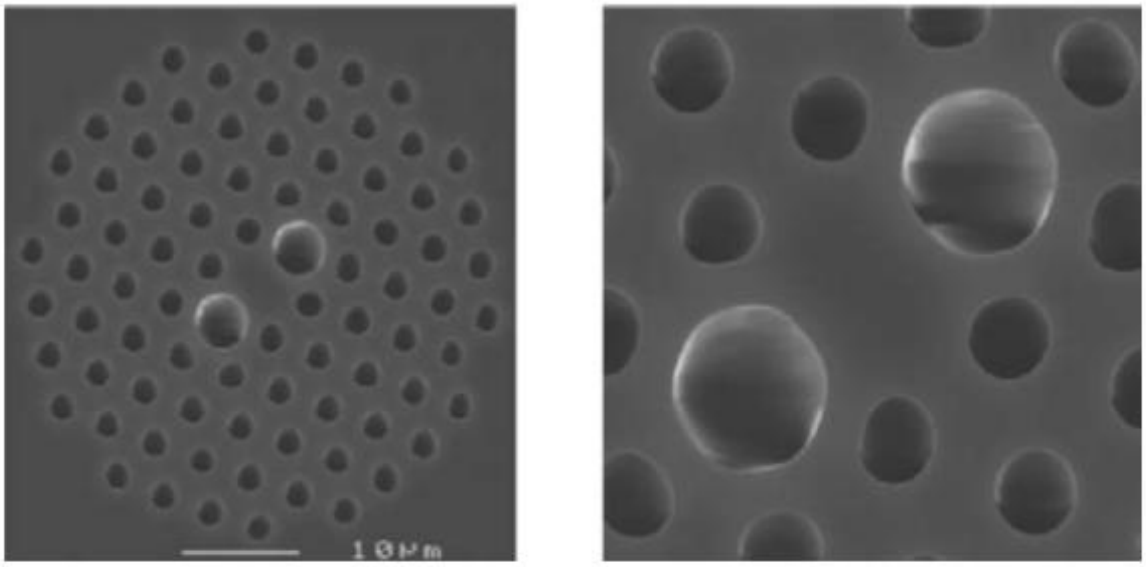

Fig. 3.5: Microscope picture of (a) the cross-section and (b) the core region of a highly birefringent triangular optical fiber [42].

Birefringence is deliberately introduced in polarization maintaining (PM) waveguides [43] which can be implemented in many THz schemes such as polarization-sensitive THz time-domain spectroscopy [44]. Generally, high-birefringence is obtained in a PCF by breaking the symmetry of either the core [45] or the holey cladding [46]. These protocols led the way to some excellent reports on the polarization maintaining THz optical fibers [47]–[49].

Birefringence is responsible for the phenomenon of double refraction whereby a ray of light, when incident upon a birefringent material, is split by polarization into two rays taking slightly different paths. This effect was first described by the Danish scientist Rasmus Bartholin in 1669, who observed it in calcite, a crystal having one of the strongest birefringence. However it was not until the 19th century that Augustin-Jean Fresnel described

the phenomenon in terms of polarization, understanding light as a wave with field components in transverse polarizations (perpendicular to the direction of the wave vector).

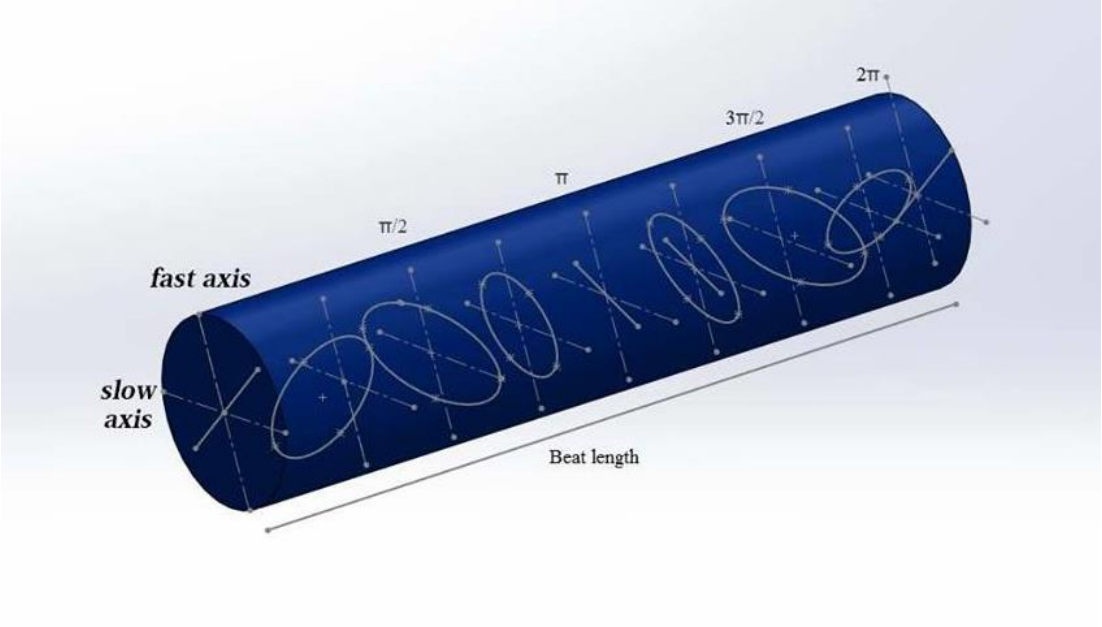

Fig. 3.6: Birefringence property of optical fibers

In optical fibers birefringence usually results from two sources:

(a) Stress birefringence,

(b) Shape or form birefringence.

Stress birefringence is results from bends and twists in the fiber. Shape or form birefringence results from unintentional deformation during fabrication. Other sources of birefringence are fiber strain, fiber side pressure etc. [50].

Effects of small birefringence are observed in conventional fibers, such as pulse spreading due to differential group delay. Large birefringence restricts the pulse spreading effects and the modes are not coupled together by bends and twists in the fiber. In this case, the energy in each mode remains constant along the fiber length. Therefore, effects of large birefringence are an advantage in PCF. PCF can be made highly birefringent by having different air-hole diameters along the two orthogonal axis or by asymmetric core design. PCF had illustrated modal birefringence of an order of magnitude higher than that of the conventional fibers [Ju et al]. Research results [Nielsen et al.] had shown that the form birefringence increases with wavelength as the mode increases in size and thereby overlaps the nonsymmetrical air/glass boundary.

3.2.1 Polarization Properties of Optical Fiber

In standard fiber transmission systems, imperfections in the core-cladding interface introduce random birefringence that leads to light being randomly polarized. Conventional circularly symmetric optical fibers do not maintain the polarization state of the guided mode along their length. Although they are nominally isotropic, small twists, bends, and other stresses impose unknown and uncontrolled birefringence on the fiber, so the polarization of the fiber output is unpredictable. These problems with random birefringence are in PMFs overcome by deliberately introducing a larger uniform birefringence throughout the fiber. Current PMFs, such as PANDA or Bow-tie fibers [51], achieve this goal by applying stress to the core region of a standard fiber, thereby creating a modal birefringence up to Δn~5.10−4. [52, 53]. The polarization beat length L_B is a measure of the birefringence and is defined as [54]-

$$L_B = \frac{2x}{\beta_x - \beta_y} = \frac{\lambda}{n_x - n_y} \tag{3.11}$$

Where, and β_y are the propagation constants of the two modes and n_x and $n_y$are the refractive index that each mode sees, with shorter L_B corresponding to stronger birefringence.

3.3 Loss Mechanisms in Optical Fiber

The most important factor for any optical fiber technology is loss. Losses in conventional optical fibers have been reduced over the last 30 years, and further improvement is unlikely to be reached. Implementing porous air core in a PCF instead of solid rod came out as a solution. Use of a porous core is resulted in reduction of quantity of solid material in the core as well as the absorption loss. Efficient honeycomb band-gap fibers were reported [55, 56] where porous core PCFs were investigated both numerically and experimentally. Also, a hexagonal PCF with hexagonal porous core (hexa-core) was reported [57] with a low absorption loss (0.12 cm^{-1}) where Teflon was used as the background material. Following, a better approach with Topas was presented which had an octagonal porous core (octa-core) inside an octagonal cladding [58] with a lessened loss (0.07 cm^{-1}) resulted due to the lower bulk material absorption loss of Topas. This limit is important, since it sets the amplifier spacing in long-haul communications systems, and thus is a major cost of a long-haul transmission system [59].

The optical loss α_{dB}, measured in dB/km, of PCFs with a sufficiently reduced confinement loss, can be expressed as

$$\alpha_{dB} = \frac{A}{\lambda^4} + B + \alpha_{oH} + \alpha_{iR} \tag{3.12}$$

Where, A, B, α_{OH} and α_{IR} the Rayleigh scattering coefficient, the imperfection loss, and OH and infrared absorption losses, respectively. At the present time the losses in PCFs are dominated by OH absorption loss and imperfection loss [60]. Losses in hollow-core fibers are limited by the same mechanisms as in conventional fibers and in index-guiding PCFs, that is absorption, Rayleigh scattering, confinement loss, bend loss, and variations in the fiber structure along the length. However, there is the possibility to reduce them below the levels found in conventional optical fibers, since the majority of the light travels in the hollow core, in which scattering and absorption could be very low.

3.3.1 Confinement Loss:

In the conventional fiber optics, the diversity of refractive index between core and cladding causes confinement of light in the fiber core. The same thing happens in the index guiding mechanism in PCFs. The core refractive index (n_{core}) is greater than the average refractive index of the cladding (n_{clad}), and light is guided by a modified form of internal reflection, which is usually referred to the modified total internal reflection (MTIR) guiding mechanism. Small-core holey fibers (HFs) can offer tight mode confinement, and are, therefore, attractive for highly nonlinear fiber applications. However, we show here that confinement loss can significantly degrade the performance of devices based on such small core fibers.

The basic loss mechanisms in PCFs are absorption by impurities [61], scattering on air/glass interface, structural non uniformity, micro and macro-bending loss [62] and confinement loss [63]. The confinement mechanisms can be thought of as being produced by the existence of a homogeneous material with a specific average index [64]. In single material PCFS, guided modes are inherently leaky because the core index is the same as the index of the outer cladding without air holes [65]. The effective index (n_{eff}) is a complex value and its imaginary part Im (n_{eff}) is related to losses through the equation [66]

$$L = \frac{40\pi . \mathrm{Im}(n_{eff}) \times 10^{6}}{\lambda[um] . \ln(10)} \qquad (3.13)$$

So, the confinement loss is determined by the geometry of the PCF, especially air holes formation in the cladding. Confinement loss is a harmful parameter in optical telecommunication systems. It can attenuate optical pulses through the fiber. It can also decrease the performance of the PCF in nonlinear applications [67].Producing low-loss holey fibers requires careful thought. The effect of the confinement loss can be reduced by doping the core region, which also increases nonlinear refractive index of the glass and reduces splice loss. In single-material holey fibers, light can always leak out to the cladding. Increasing the number of rings of holes is one way to reduce the confinement loss [68].

3.4.2 Effective Material Loss (EML):

To investigate the loss property of a THz waveguide, researchers introduce a parameter called the effective mode loss which is defined by Nielsen et al.

$$\alpha_{eff} = \frac{\alpha_{mode}}{\alpha_{mat}} = \frac{1}{2}\left(\frac{\in_0}{\mu_0}\right)^{\frac{1}{2}} \frac{\int_{mat} n_{mat} |E|^2 \, dA}{\left|\int_{all} s_z dA\right|} \tag{3.14}$$

Where, α_{mat} is the material absorption loss, n_{mat} is the refractive index, α_{mode} is the fundamental mode loss and $\in_0$ and μ_0 are the permittivity and permeability of free space, respectively. S_z is the pointing vector of the z-component and $s_z = \frac{1}{2}\vec{E} \times \vec{H}.Z$, where E and H are the electric and magnetic fields, respectively. Integration in the numerator of Eq. is performed only over the solid material region. EML changes when the frequency and core diameter changes. EML increases with the increase of core diameter because more material is used as the size of the core increases.

Bending Loss:

Various theoretical methods exist to predict curvature loss in optical waveguides. The usual approach is to use a simplified formula introduced by Marcuse, applicable to weakly guided waveguides, including most optical fibers, for sufficiently large radii of curvature. This formula agrees well with experiment for single-mode fiber, after adjustments are made for bend-induced stress. However, for multimode fiber it can be quite inaccurate as it overestimates bend loss at a large amount. Other analytical bend loss formulae are similarly limited, in that none are known to reliably predict bend loss in multimode fibers. This has become a significant problem with the development of the coiled multimode fiber amplifier, which uses bend loss to strip out the higher order fiber modes, and thereby achieve single-mode, large mode area operation. Optimizing these devices, and understanding their ultimate limitations, requires that mode-dependent bend loss be predicted accurately. A modification of Marcuse's simplified bend loss formula is suggested by Schermer but it underestimates the bend loss at a similar large amount for multimode fibers. Though the authors identified the reason behind this, the remedy against requires a simulated data which weakens the justification of using an analytical formula. Thus, a formula for predicting bend loss for multimode fibers having greater accuracy is worth developing.

The simplified bend loss formula (the word 'simplified' indicates that this formula is a simplified form of a more complex one) for step index optical fibers reported by Marcuse is as follows,

$$2\alpha = \frac{\pi^{\frac{1}{2}} k^2 \exp\left(-\frac{2\gamma^3 R}{3\beta_z^{\,2}}\right)}{2R^{\frac{1}{2}}\gamma^{\frac{3}{2}} V k_{m-1}(\gamma a) k_{m+1}(\gamma a)} \tag{3.15}$$

Here, a is the core radius, 2α is the power loss coefficient, κ and γ are the field decay rates in the core and cladding defined as,

$$k = \sqrt{k_{core}^2 - \beta_z^2} \tag{3.16}$$

$$\gamma = \sqrt{\beta_z^2 - k_{clad}^2} \tag{3.17}$$

and the K terms are modified Bessel functions, V is the normalized frequency, k_{core} is the core propagation constant, k_{clad} is the cladding propagation constant and β_z is the effective propagation constant of the fundamental mode (the z- axis being the direction of propagation). Bend loss in units of dB/length is obtained by multiplying 2α by the factor 4.343.

CHAPTER 4
Design of Proposed PCFs

Two conventional design of PCF has been shown in our thesis. One of the proposed model has an octagonal lattice in the cladding region and asymmetry in the core region where three parameters such as, pitch, air hole diameter and number of air hole rings, can be varied to obtain useful properties. This proposed model has the property of high birefringence and flattened dispersion. On the contrary, the other proposed model has an octagonal lattice structure in the cladding region and hexagonal lattice structure in the core region. This proposed model exhibits low loss properties of optical fiber. This models of PCF are shown in this chapter.

4.1 A Novel Design of Highly Birefringent Flattened Dispersion PCF:

In this section we proposed a novel micro-structured photonic crystal fiber structure with air holes of the cladding are arranged in an octagonal lattice structure and core is asymmetric by introducing rows of small sized holes. One usually designs various kinds of waveguides to guide the THz wave because the material absorption loss is high in THz band. One of the lowest material loss materials is dry air in the THz frequency range. It has been reported that the mode field extends into the low index air cladding region when a dielectric rod is surrounded by air and is operating very close to its cutoff frequency. Today, photonic crystal fiber (PCF) is the most popular optical fiber but in case of a solid core, the material absorption loss is too high and is almost equal to the bulk absorption loss of the material. Due to this fact, we design a porous-core octagonal PCF to overcome the above mentioned problems. To significantly reduce the material loss, a larger air filling fraction (AFF) is used. In our design, we use five air hole rings for the cladding region.

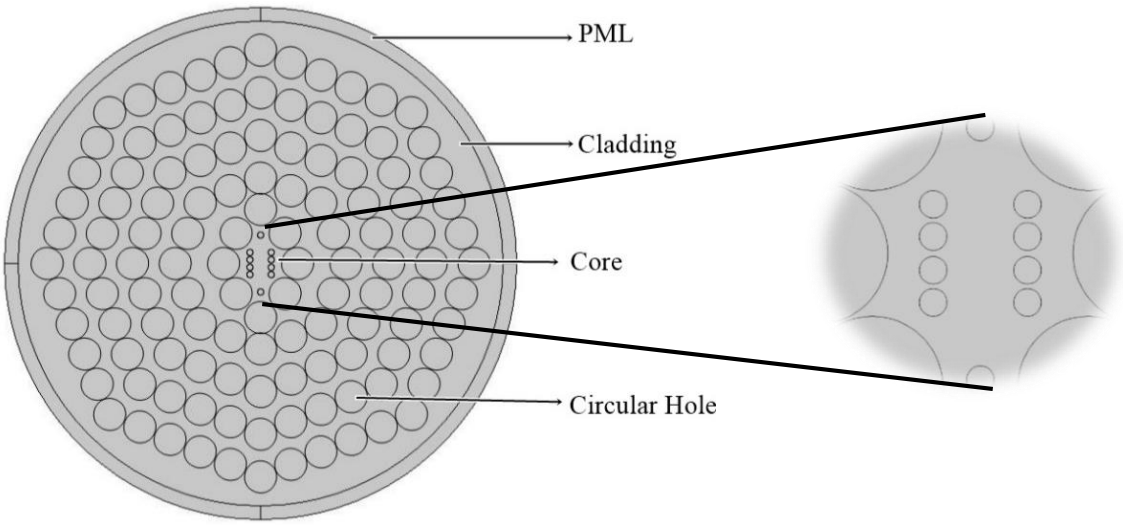

Fig. 4.1**:** Cross section of a Highly Birefringent Flattened Dispersion PCF

The cladding part is formed by a distribution of sub-wavelength sized air holes on the background of cyclic olefin copolymer (namely, TOPAS). This material has an almost constant refractive index of 1.5258 in the 0.1-1.5 THz range [69]. Also, low bulk material loss, insensitivity to humidity [70], and high glass transition temperature due to different grades of constituents [71] etc. makes it a very suitable material for PCF fabrication.

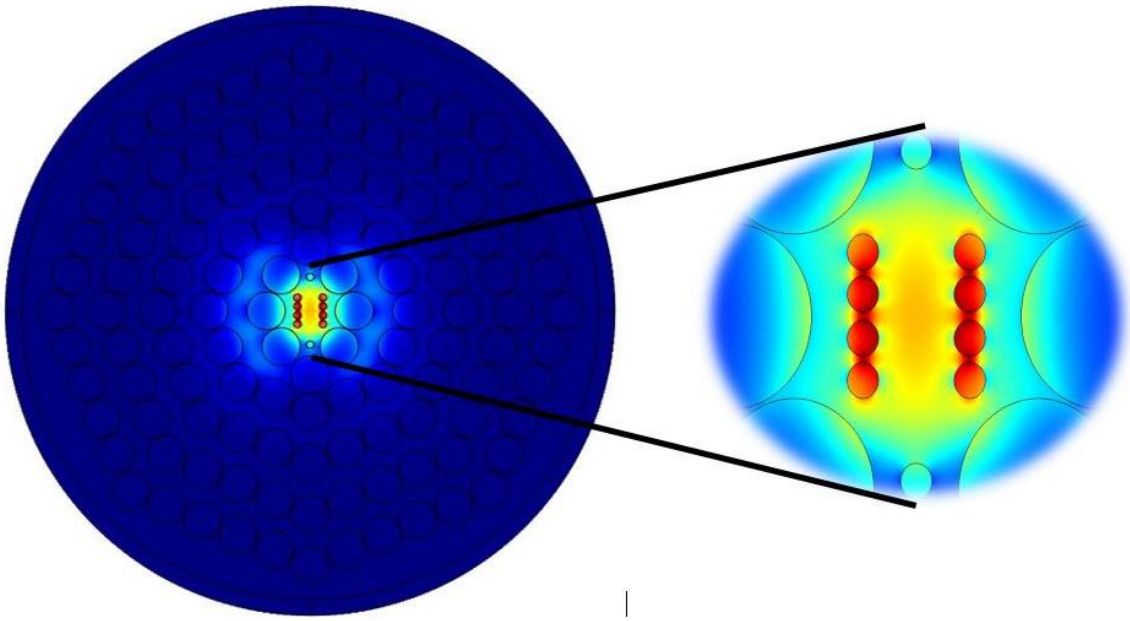

Fig. 4.2**:** Electric field distribution (x polarized) of the proposed PCF

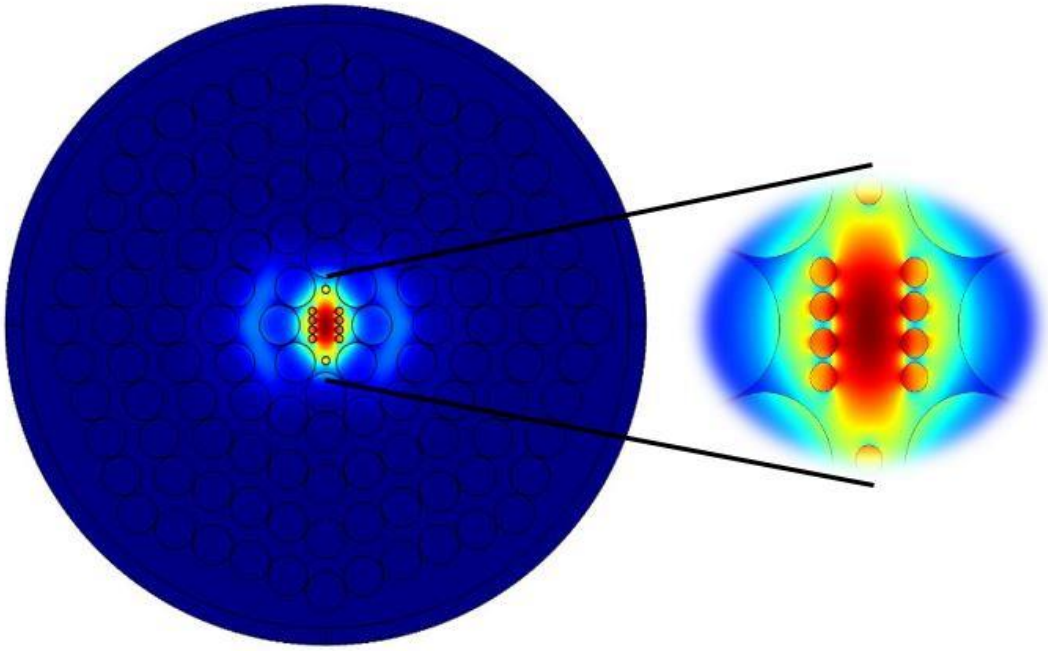

Fig. 4.3: Electric field distribution (y polarized) of the proposed PCF

4.1.1 Design Approach:

Figure 4.1 shows the topology cross section, and Fig. 4.2, 4.3 depicts the power flow distribution of the designed micro-structured octagonal photonic crystal fiber. An octagonal lattice structure is chosen due to the better confinement and 1.32 times more air holes than the hexagonal PCF, which can better reduce the material absorption loss. The term porosity, which is determined by the size of the holes at the core, is defined as the ratio of air hole area to the cross section area of the core. As air holes in the core act as a low index material and dry air is transparent in the THz frequency range, material absorption loss can be significantly reduced. This design is based on the total internal reflection at the core. The core diameter, $D_{core}= 2(\Lambda-d/2)$ has been changed while AFF is kept fixed at 0.75 throughout all numerical calculations, where d denotes the diameter of the air holes at the cladding region and Λ is the distance between two adjacent air holes. We have been varying d and Λ while maintaining AFF at value 0.75 for various core diameter and frequencies. For a particular Dcore, the porosity at the core can be obtained by varying the air holes diameter.

Asymmetry is created in the core region by introducing rows of small sized holes with diameter D_{core}. The holes are spaced at a horizontal distance L_x from the center and with uniform spacing L_y between each other. Two other same sized holes are also placed in the first cladding ring. Aside from inducing birefringence, all these small sized holes transmit a

significant portion of the confined mode energy and thus help in reducing the effective material loss caused by index guiding in the material.

Fig. 4.2 shows the tightly confined electric mode field patterns of the two orthogonally polarized modes at 1 THz. The key properties have been investigated using full vector finite element method (FEM). To prevent reflection and back-scattering, perfectly matched layer (PML) has been employed at the circular boundary.

4.2 A Novel Design of Low Loss PCF:

In this section we want to propose a novel micro-structured photonic crystal fiber structure with air holes of the cladding are arranged in an octagonal lattice structure and air holes of core are arranged in hexagonal lattice structure. The whole PCF is based on cyclic-olefin copolymer (COC), which is commercially known as TOPAS. This material has an almost constant refractive index of 1.5258 in the 0.1-1.5 THz range. Compared to other polymer materials (such as PMMA, HDPE, PP etc.), TOPAS provides few definite advantages. Also, low bulk material loss, insensitivity to humidity, and high glass transition temperature due to different grades of constituents etc. makes it a very suitable material for PCF fabrication.

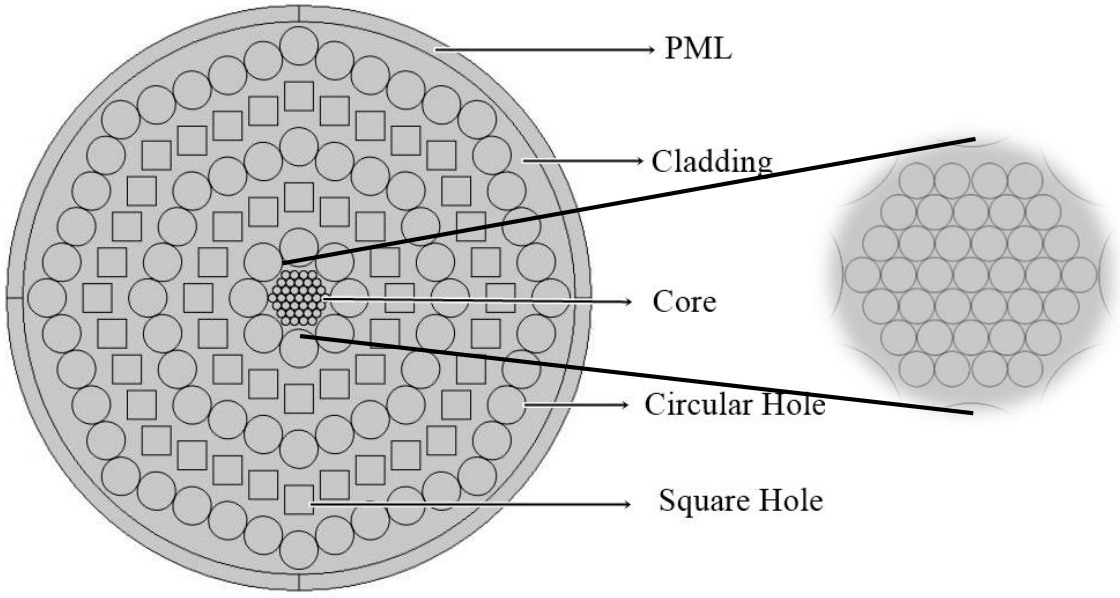

Fig. 4.4**:** Cross section of the proposed low loss PCF

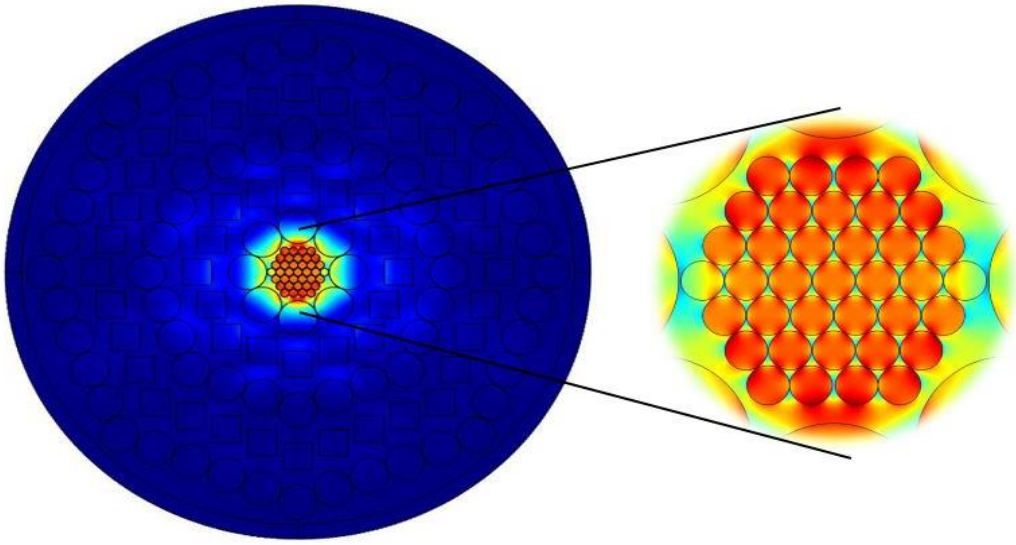

Fig. 4.5: Electric field distribution of the proposed PCF

4.2.1 Design Approach:

Figure 4.4 shows the topology cross section, and Fig. 4.5 depict the power flow distribution of the designed micro-structured octagonal photonic crystal fiber. It can be observed from Fig. 4.16 that two different types of circular lattices are used for the core and cladding. An octagonal lattice structure is chosen due to the better confinement and 1.32 times more air holes than the hexagonal PCF, which can better reduce the material absorption loss. Meanwhile, the core air filling fraction was variable and was mostly determined by the porosity. Porosity is a common term used in porous core fiber discussions, defined as the ratio between air-hole areas to the total core area. As air holes in the core act as a low index material and dry air is transparent in the THz frequency range, material absorption loss can be significantly reduced. This design is based on the total internal reflection at the core. The core diameter, $D_{core}= 2(\Lambda-d/2)$ has been changed while AFF is kept fixed at 0.76 throughout all numerical calculations, where d denotes the diameter of the air holes at the cladding region and Λ is the distance between two adjacent air holes. We have been varying d and Λ while maintaining AFF at value 0.76 for various core diameter and frequencies. For a particular D_{core}, the porosity at the core can be obtained by varying the air holes diameter.

The core part is formed by a triangular lattice distribution of sub-wavelength sized air holes. All the holes in the core have a diameter d_c. The one used in the core has six air holes in the first ring and six added air holes in every added ring. Fig. 4.5 shows the tightly confined electric mode field patterns of the proposed model at 1 THz. The key properties have been investigated using full vector finite element method (FEM). To prevent reflection and back-scattering, perfectly matched layer (PML) has been employed at the circular boundary.

CHAPTER 5

Analysis & Results

We have investigated the dispersion, power fraction, birefringence and loss properties of the designed novel structures using the FEM approximation. In this section we discuss the flexibility of different design parameters & their impact on the above mentioned properties. Depending on the application, different kinds of optimization can be preferred.

At the very beginning, three things are to be kept in mind while designing efficient optical THz waveguides: (1) material absorption loss (2) confinement loss and (3) power fraction in the air core. The variable parameters: porosity, D_{core}, and f are chosen on the basis of the three major things mentioned above.

5.1 Analysis for Highly Birefringent and Flattened Dispersion PCF:

Our optimum core diameter is chosen at 250 um and operating frequency is 1 THz for this design.

Effective Refractive Index:

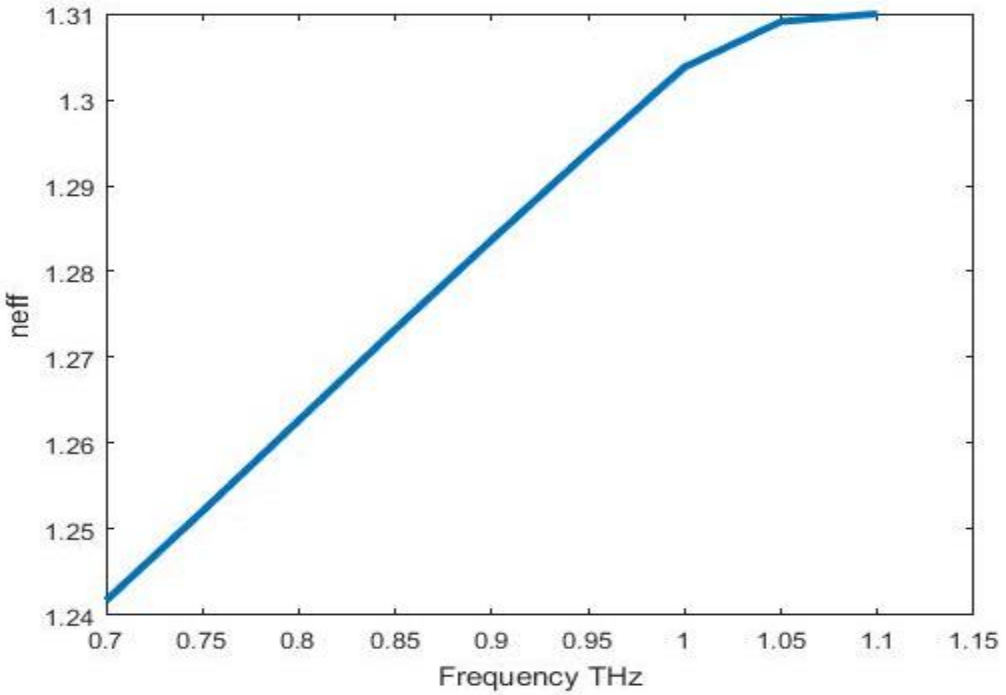

Fig. 5.1: Effective refractive index vs. frequency

From Fig. 5.1, it can be observed that effective refractive index is scaled up at higher values of frequency.

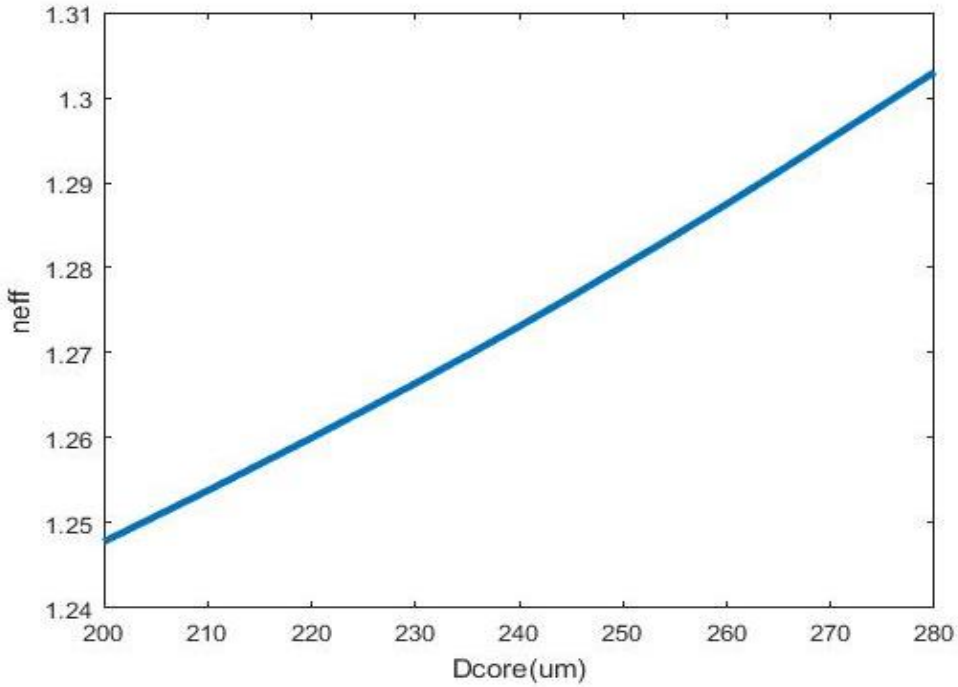

Fig. 5.2: Effective refractive index vs. core diameter

From Fig. 5.2, it can be observed that effective refractive index is scaled up at higher values of core diameter.

V parameter:

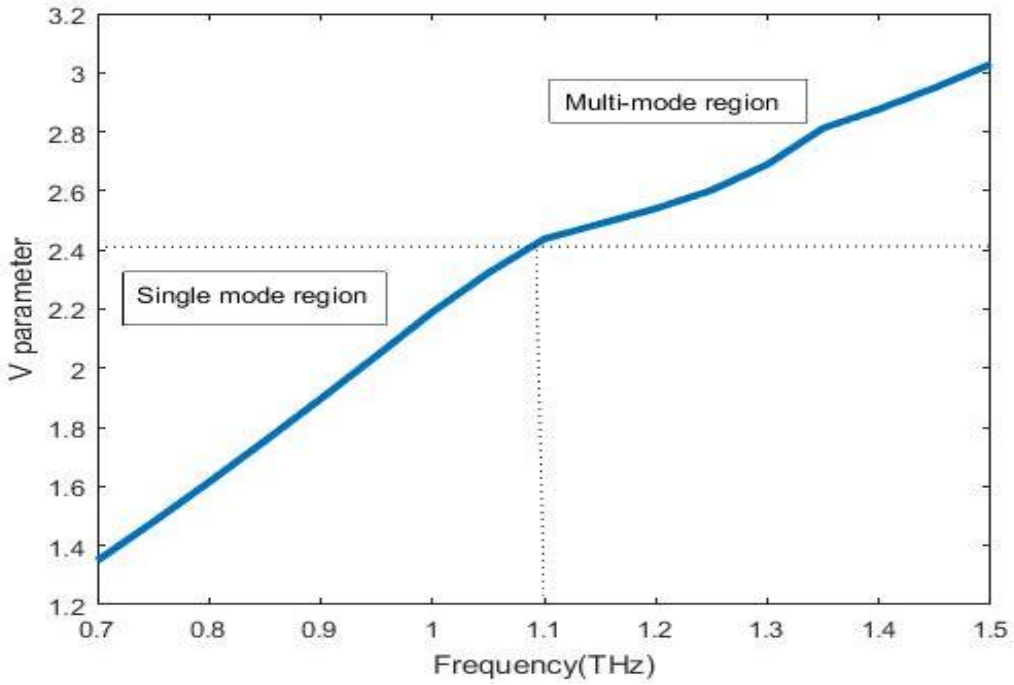

Fig. 5.3: V parameter vs. frequency

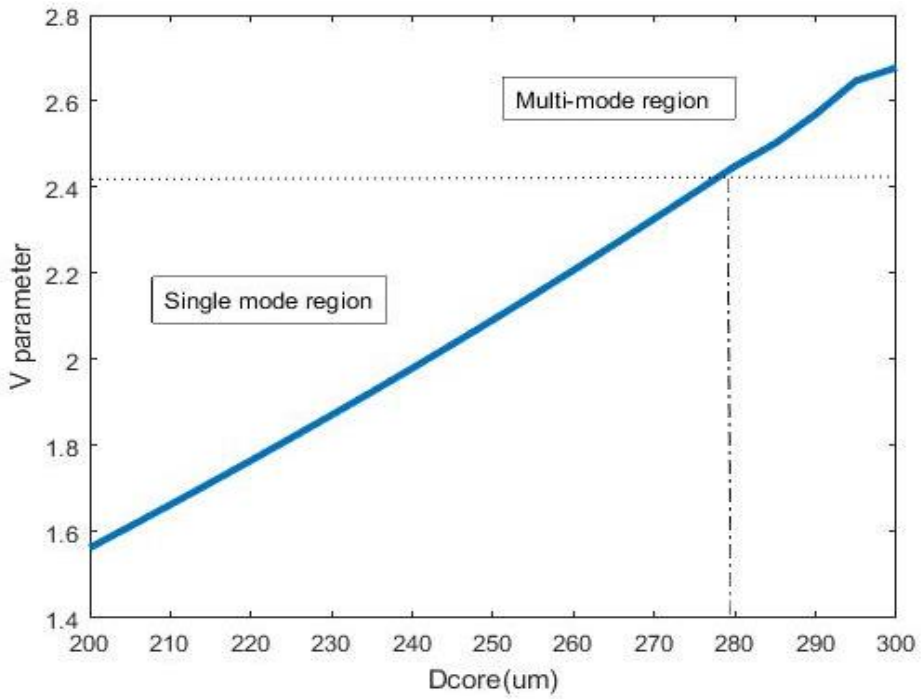

Fig. 5.4: V parameter vs. D_{core}

We know that V parameter cannot be more than 2.405, which is graphically presented in Fig. 5.3, 5.4 where the x-axis of Fig. 5.3 represents the frequency while the x axis of Fig. 5.4 represents the D_{core}. It can be observed that the V parameter increases with both of the independent variables. From Fig.5.3, 5.4, it can be approximated that single-mode exists when $D_{core} < 279$ μm and $f < 1.1$ THz, which is implied in the following numerical analyzes.

Effective Material Loss (EML):

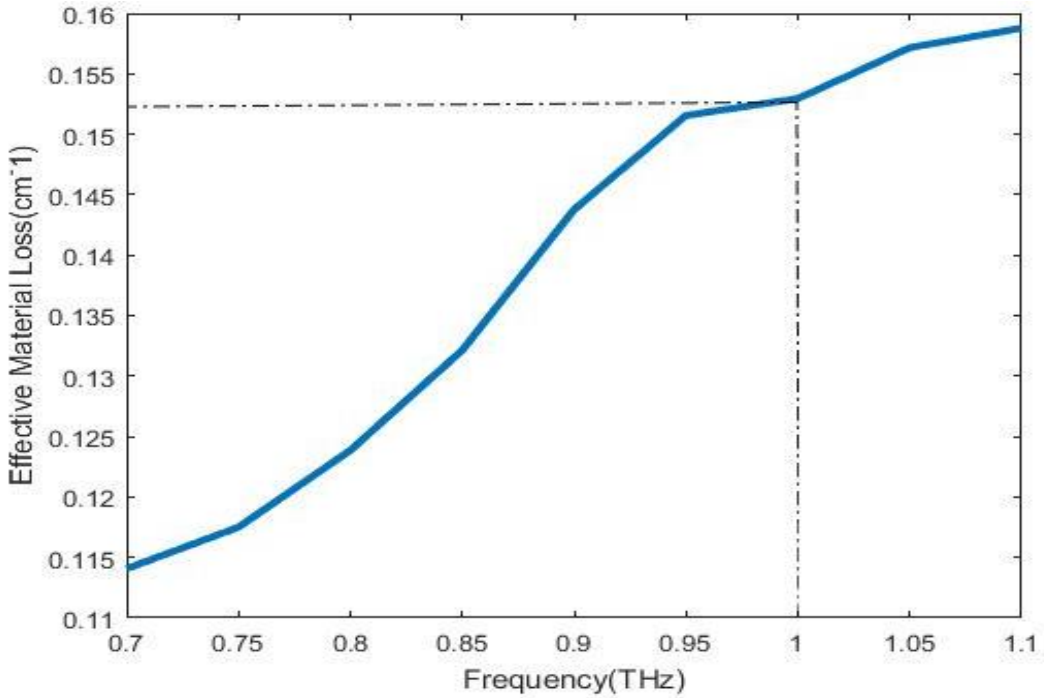

Fig. 5.5**:** EML vs. frequency

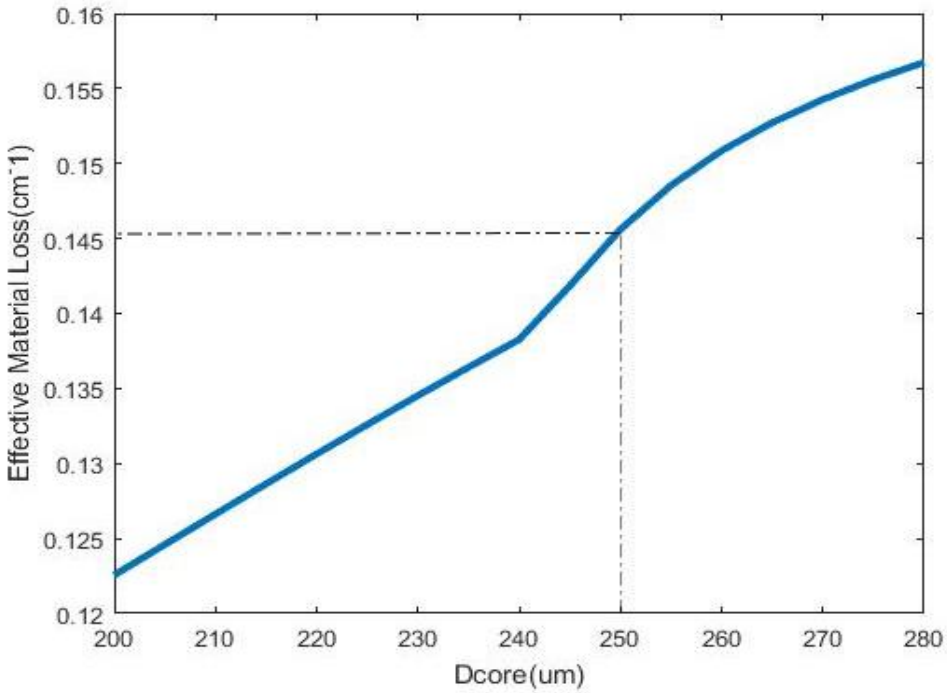

Fig. 5.6: EML vs. D_{core}

Fig. 5.5, 5.6 represents the effective material loss (EML) as a function of frequency and diameter of the core. We can see a significant change of EML when the frequency and core

diameter changes. EML increases with the increase of core diameter because more material is used as the size of the core increases. Again with the increase of frequency EML increases. At 1 THz, EML is about 0.153 cm^{-1} and at D_{core}= 250 um, EML is about 0.146cm^{-1}.

Confinement Loss:

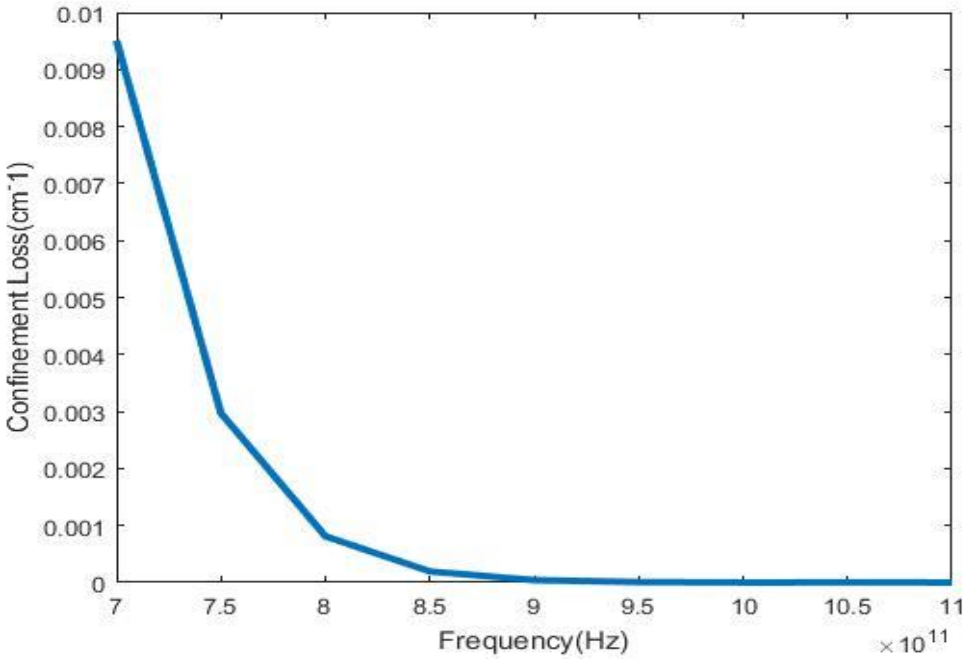

Fig. 5.7: Confinement loss vs. frequency

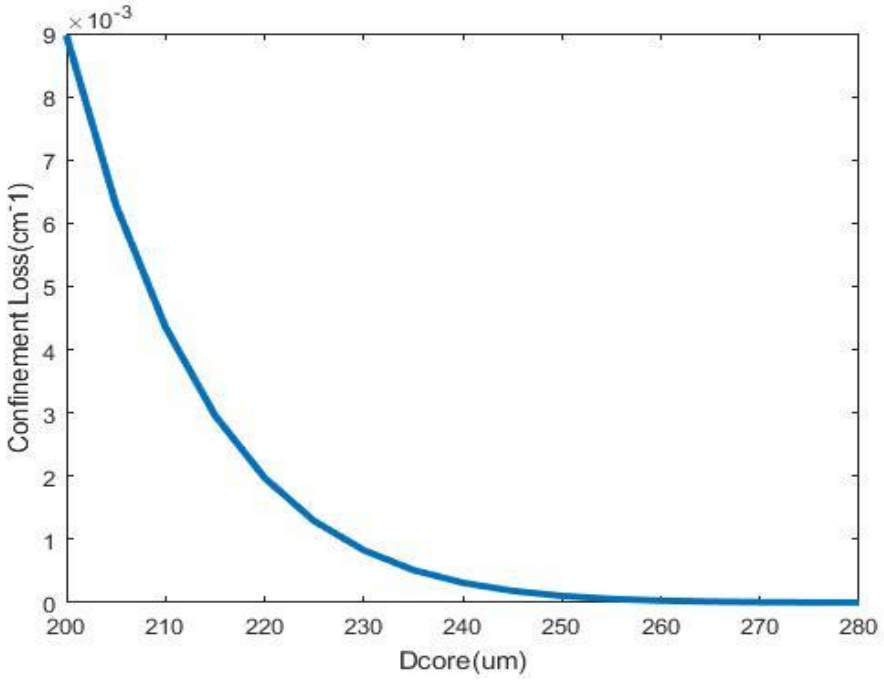

Fig. 5.8: Confinement loss vs. D_{core}

Fig. 5.7, 5.8 shows confinement loss as a function of frequency & core diameter. It can be observed that confinement loss is scaled down at higher values of frequency and core diameter. It is due to the fact that the extended core diameter and frequency difference between refractive indices of core and cladding is increased. As a result the enlarge index difference helps confining the light more inside the core and reduces the loss. At f = 1 THz and $D_{core} = 250$ um, confinement loss is about $0.0004 cm^{-1}$.

Dispersion:

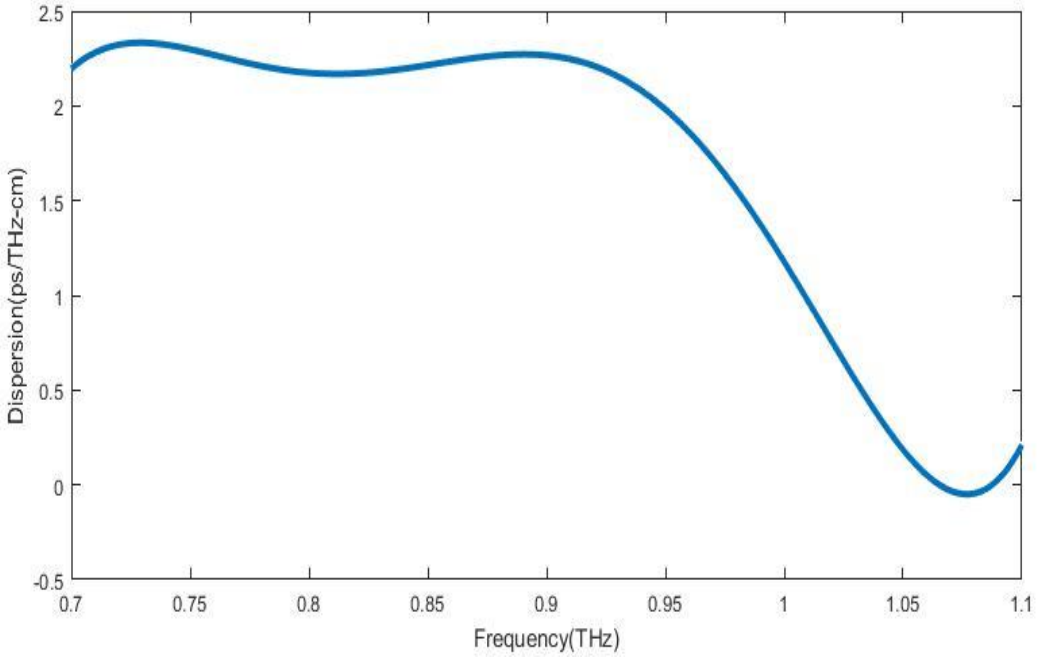

Fig. 5.9: Dispersion vs. Frequency

From the Fig. 5.9, it is observed that the fiber doesn't fluctuate from its equilibrium position within 0.7 to 0.95 THz. So it can be said that the designed fiber is a flattened dispersion fiber of 2.2 ± 0.09 ps/THz/cm.

Power Fraction:

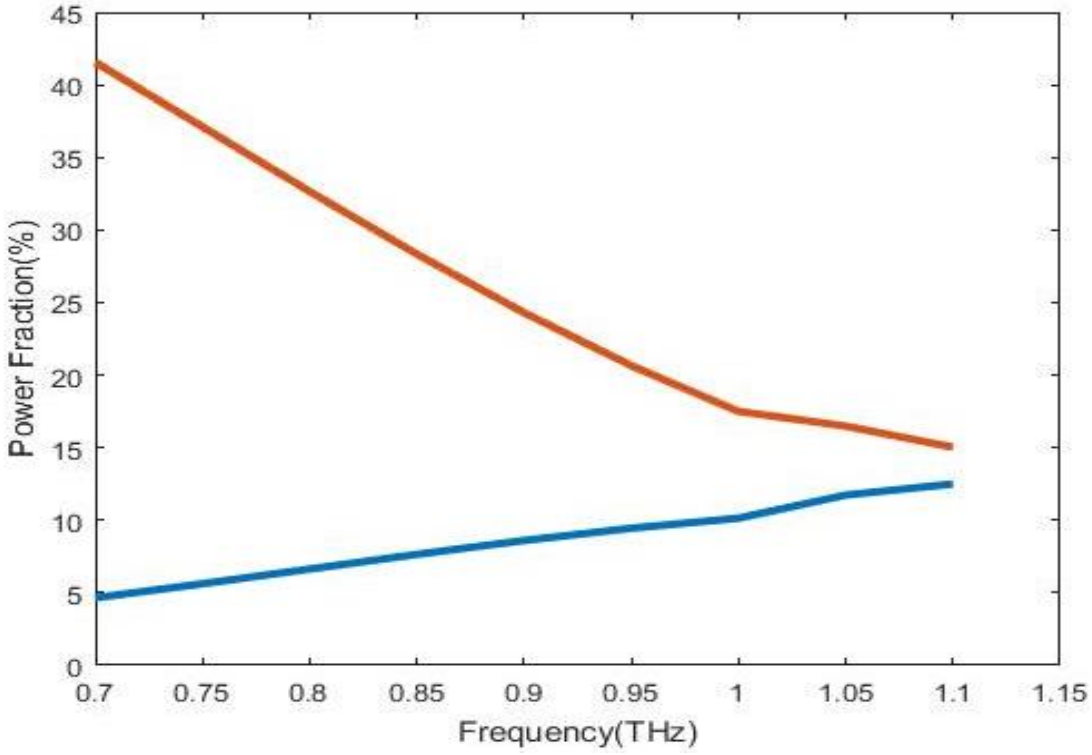

Fig. 5.10: Power fraction in core and cladding vs. frequency

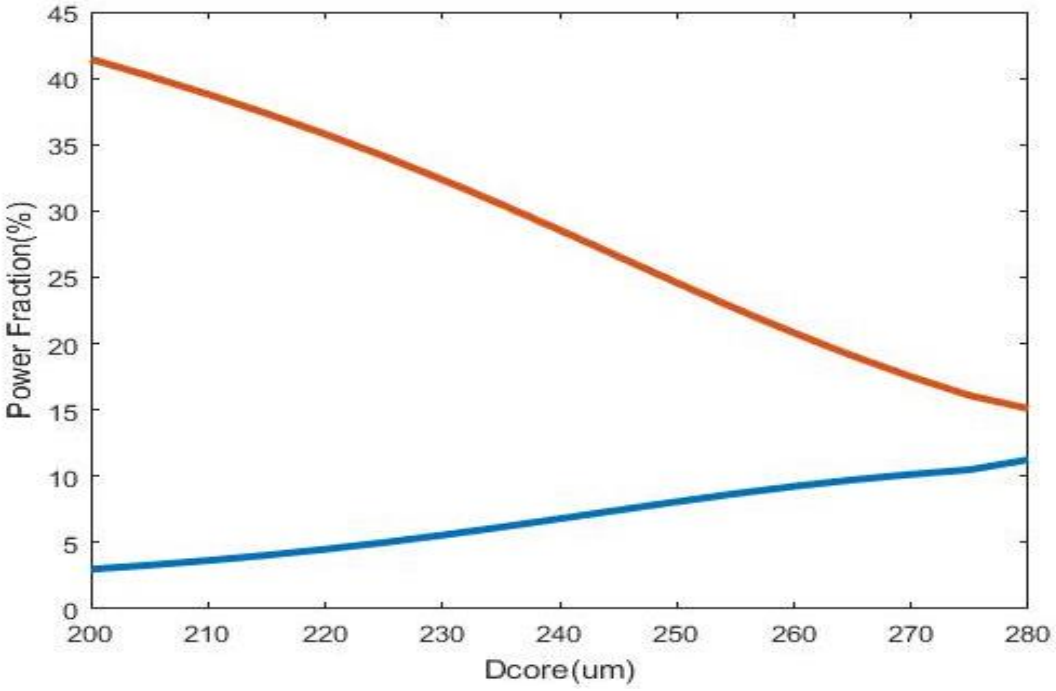

Fig. 5.11: Power fraction in core and cladding vs. core diameter

Fig. 5.10, 5.11 shows the power flow distribution of the proposed PCF at optimal parameters where it can be observed, especially with the aid of the enlarged view in the inset, that for a specific effective mode index, light is well confined around the porous core. As material in core is kept much more than any other design so power fraction in core is low and EML is high.

Birefringence:

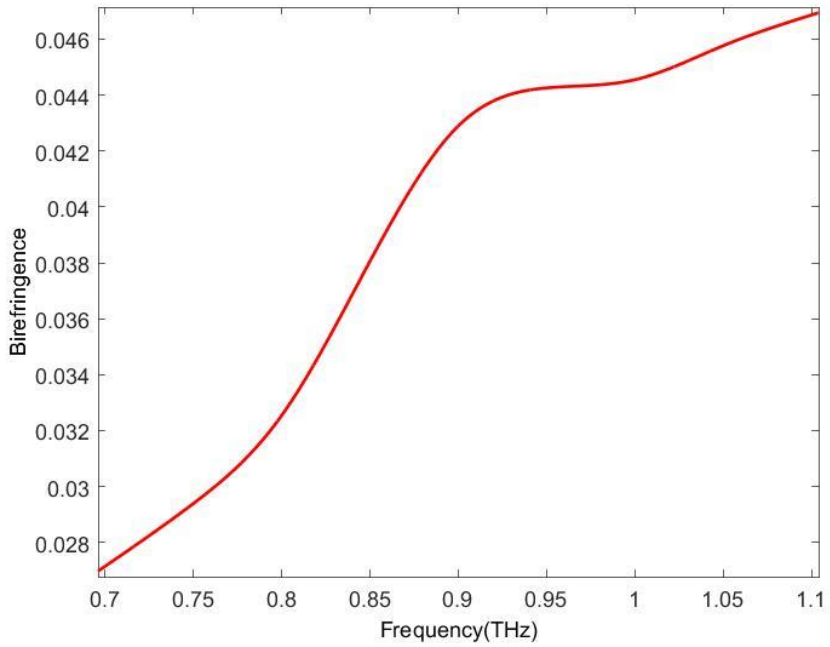

Fig 5.12: Birefringence vs. frequency

From the above Fig. 5.12 we can see the birefringence of the proposed PCF. Here birefringence increases with the increase in frequency. At 1 THz we got birefringence about 0.045.

5.2 Analysis for Low Loss PCF:

The variable parameters: porosity, D_{core}, and f are chosen on the basis of the three major things mentioned above. Our optimum core diameter is chosen at 325 um and operating frequency is 1 THz for this particular design.

Effective Refractive Index:

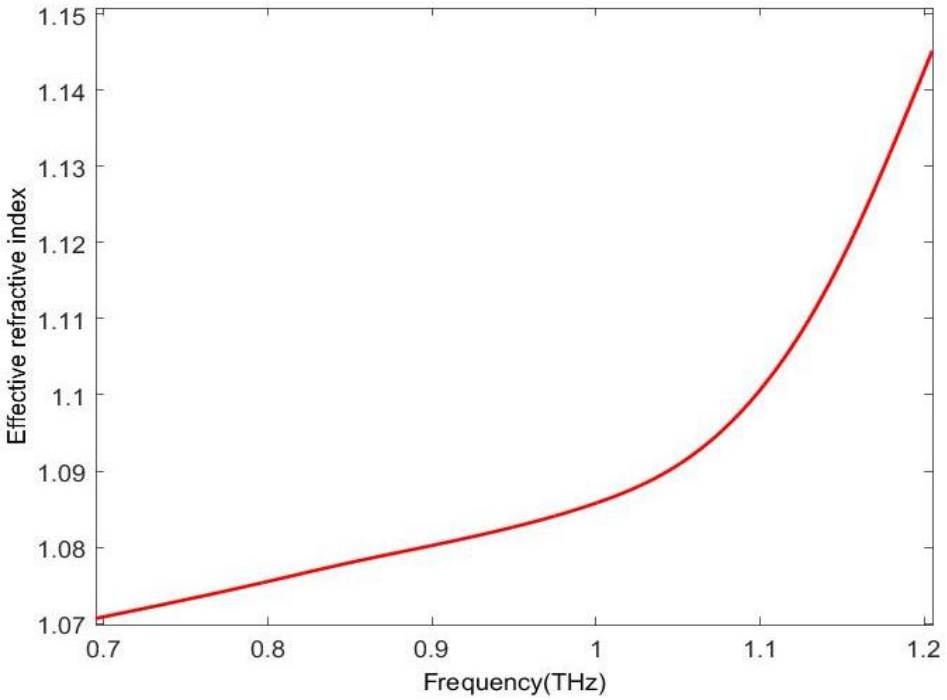

Fig. 5.13: Effective refractive index vs. frequency

From Fig. 5.13 it can be observed that effective refractive index is scaled up at higher values of frequency.

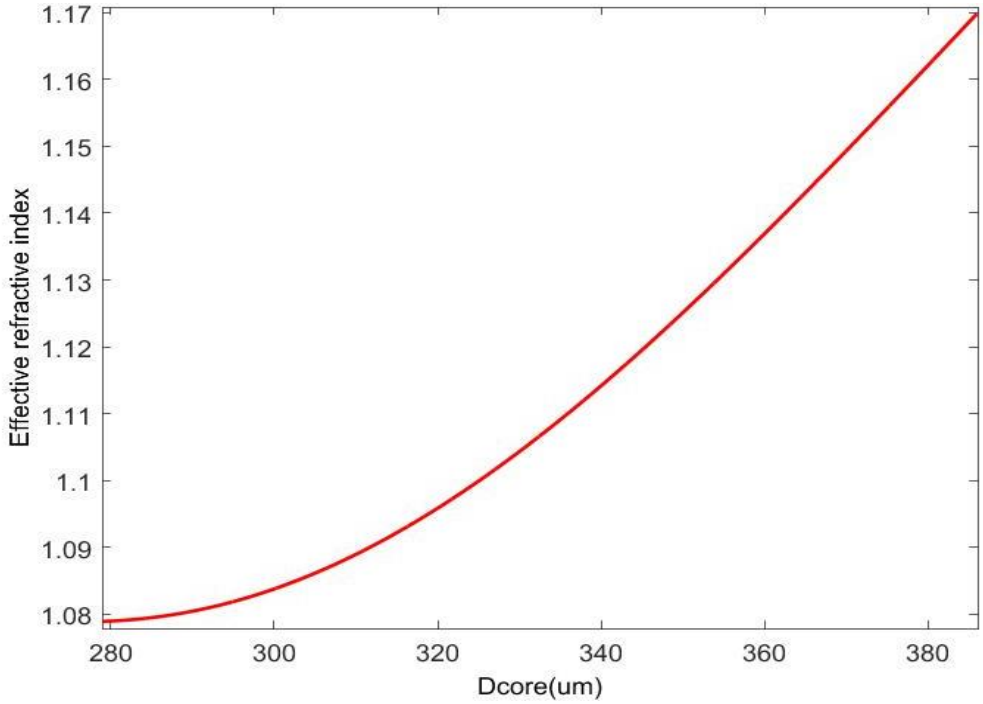

Fig. 5.14: Effective refractive index vs. D_{core}

From Fig. 5.14, it can be observed that effective refractive index is scaled up at higher values of core diameter

V Parameter:

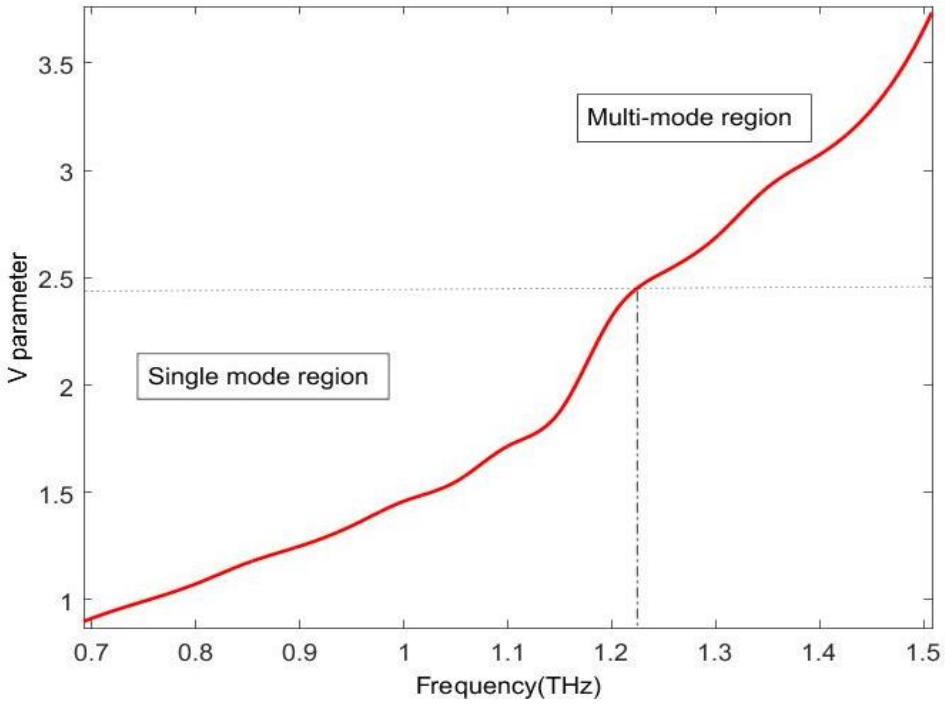

Fig. 5.15: V parameter vs. frequency

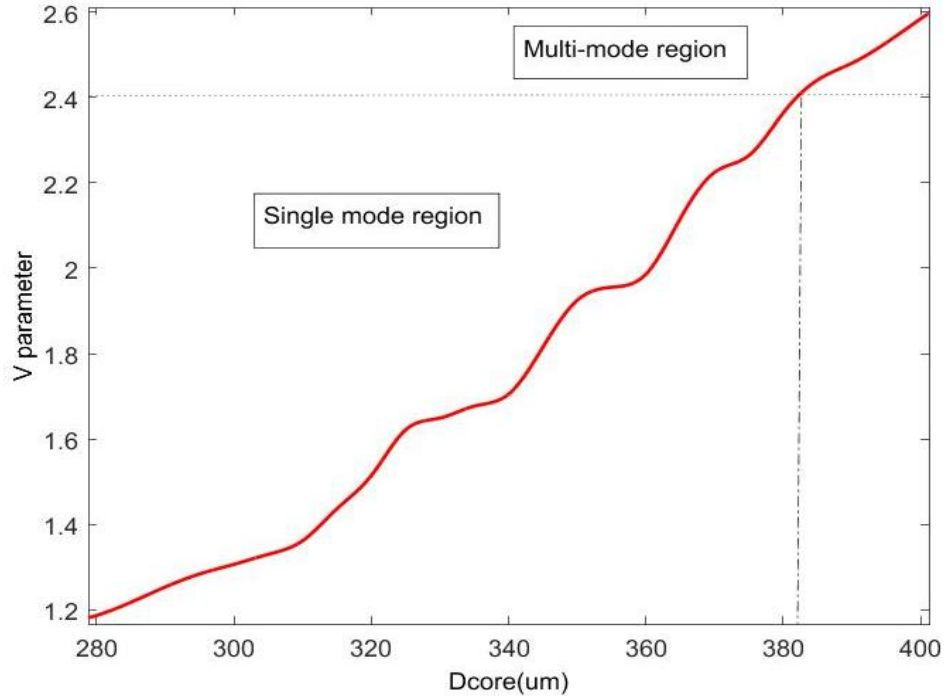

Fig. 5.16: V parameter vs. D_{core}

We know that V parameter cannot be more than 2.405, which is graphically presented in Fig. 5.15, 5.16 where the x-axis of Fig. 5.15 represents the frequency while the x axis of Fig. 5.16

represents the D_{core}. It can be observed that the V parameter increases with both of the independent variables. From Fig.5.15, 5.16, it can be approximated that single-mode exists when $D_{core} < 385$ μm and $f < 1.23$ THz, which is implied in the following numerical analyzes.

Effective Material Loss:

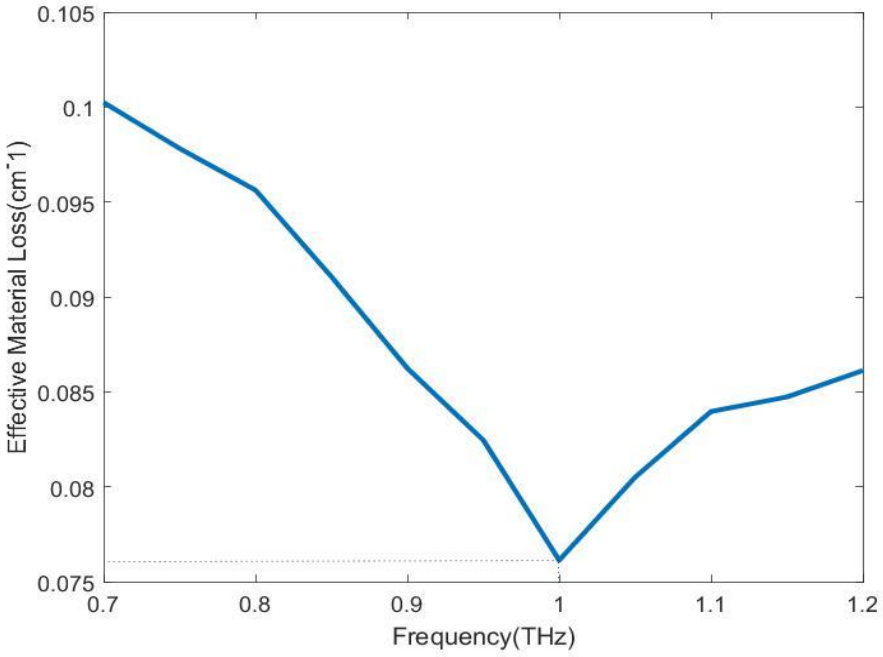

Fig. 5.17**:** EML vs. frequency

Fig. 5.17 represents the effective material loss (EML) as a function of. We can see a significant change of EML when the frequency changes. EML increases with the increase of frequency. At 1 THz, EML is about 0.076 cm^{-1}.

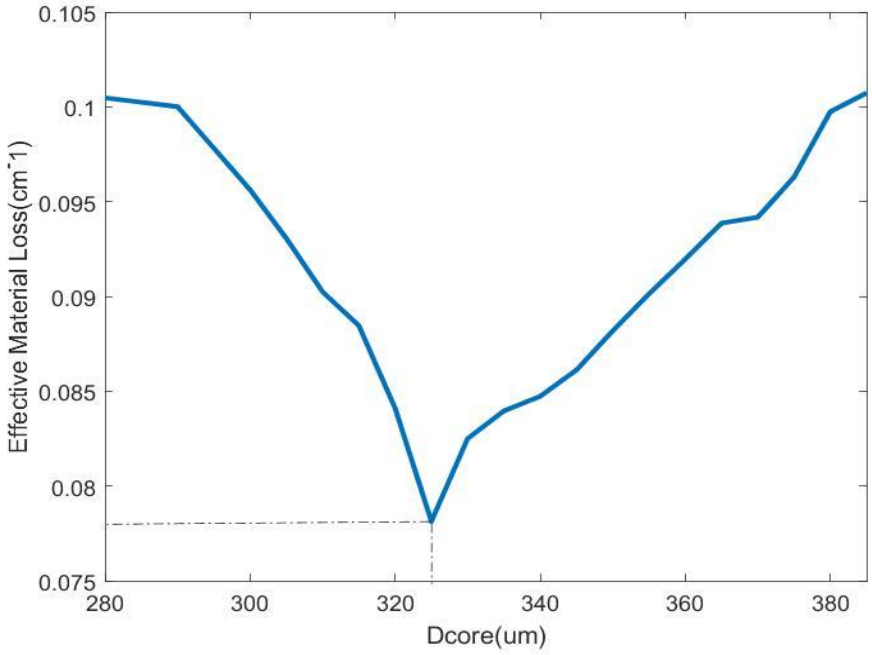

Fig. 5.18: EML vs. D_{core}

Fig.5.18 represents the effective material loss (EML) as a function of diameter of the core. We can see a significant change of EML core diameter changes. EML increases with the increase of core diameter because more material is used as the size of the core increases. EML is about 0.0775cm^{-1} at D_{core}= 325 um.

Confinement Loss:

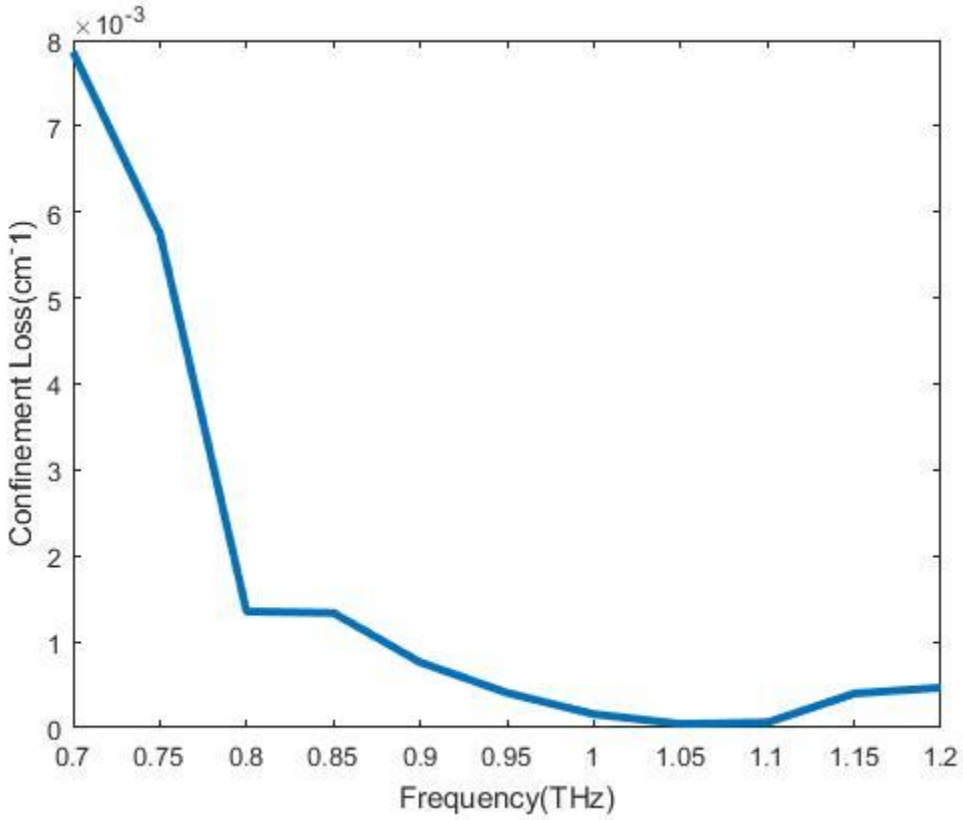

Fig. 5.19: Confinement loss vs. frequency

Fig. 5.19 shows confinement loss as a function of frequency. It can be observed that confinement loss is scaled down at higher values of frequency. It is due to the fact that the extended frequency difference between refractive indices of core and cladding is increased. As a result the enlarge index difference helps confining the light more inside the core and reduces the loss. At f = 1 THz, confinement loss is about $0.0006 cm^{-1}$.

Power Fraction:

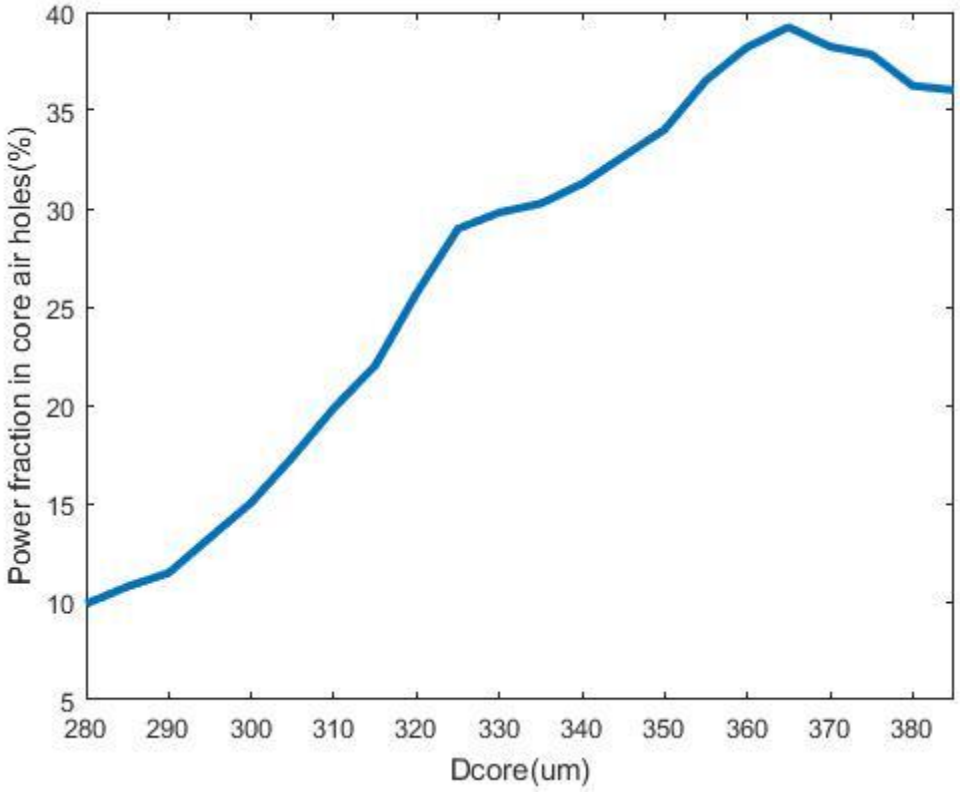

Fig. 5.20: Power fraction in core vs. core diameter

Fig. 5.20 shows the power flow distribution of the proposed PCF at optimal parameters where it can be observed, especially with the aid of the enlarged view in the inset, that for a specific effective mode index, light is well confined around the porous core.

CHAPTER 6

Conclusion

6.1 Summary:

To summarize this thesis we have demonstrated an outstanding technique for controlling the birefringence and loss properties in PCFs by introducing a pair of square holes & cicular holes in the central ring of the proposed PCF model. One of our proposed PCF model is significantly simpler than other structures proposed so far for controlling the birefringence and at the same time dispersion compensating characteristics have been obtained in the S-band (1460nm-1530nm), C-band(1530–1565 nm) and L-band (1565nm-1625nm). Other model gives us low value of loss with a high power fraction in the air holes of the core. The main conclusion of this systematic approach is that with a modest number of design parameters we could fully-tune and optimize the birefringence properties and loss properties of the PCF. The dispersion characteristics can be controlled by changing doping concentration, lattice constant and air hole diameter. Our architecture is suitable for applications as a single mode fiber, dispersion compensator.

6.2 Future Work:

Birefringence & dispersion properties of an even more asymmetric design with entire rows of air holes is going to be investigated shortly. We will calculate loss properties of the structure and compare it with our proposed structure.

Fundamental modes were focused more importantly than on other higher order modes while doing the optical characterization. Fundamental modes will have tighter confinement and less waveguide losses than the higher order modes. We are trying to investigate an analytic equation to predict the single mode behavior accurately. Moreover theoretical study on novel nonlinear phenomenon such as Intrapulse Raman Scattering, Four Wave Mixing, SCG, Temporal and Spectral Evolution, Second-Harmonic Generation and Third-Harmonic Generation is being carried out.

A novel design of birefringent fiber with flattened dispersion and low loss fiber over a broader spectrum is also in progress.

We have strong desire to investigate new medical application of PCF in near future

Appendix A

Mode Analysis Ssing COMSOL MULTIPHYSICS:

The objective of the model is to study TE waves propagating through the crystal. To model these, we used a scalar equation for the transverse electric field component Ez,

$$-\nabla.\nabla E_z - n^2 k_0{}^2 E_z = 0$$

Where, n is the refractive index and k_0 is the free-space wave number. Because there are no physical boundaries, we used perfectly matched layer as the boundary condition at all boundaries.

A.1 Modeling Instructions Model Wizard

1 Go to the Model Wizard window.

2 Click the 2D button.

3 Click Next.

4 In the Add physics tree, select Wave Optics>Electromagnetic Waves, Frequency Domain (emw).

5 Click Add.

6 Find the Studies subsection. In the tree, select Preset Studies>Mode Analysis.

7 Click Done.

Parameters:

Dcore	250[um]
f	1[THz]
dn	0.75
rn	(Dcore/pc)*sqrt(por/n)
por	0.75
p	Dcore/((1-dn/2)*2)
pc	Dcore/b
a	cos(pi/4)
r	dn*p/2
rc	rn*pc/2
L	p/4
nef	1.27
n	55

Definitions

1. In the Model Builder window, under Component 1, click Definitions and choose Perfectly Matched 1.
2. In the PML settings window, select the PML domain manually by clicking on the diagram. If a region is selected, it will turn green.

3. Set the geometry type to cylindrical.

4. Under Scaling, set the geometrical stretching type to polynomial, Scaling Factor 1, Curvature Parameter 1.

GEOMETRY 1

1. In the Model Builder window, under Component 1 right-click Geometry 1 and choose Circle.
2. In the Circle window, set the circle center at (0, 0) and radius equal to 5.8p.
3. Draw the inner circle by creating a new circle with center (0, 0) & radius 5 p. The ring between these two rings will act as PML layer.

4. Draw the inner air holes with different radii by creating new circles & changing the center positions.

5. To draw the square, choose square from Geometry 1 & change its center position.

6. Click Build All in the Property Group Settings Window. 8 Click the Zoom Extents button on the Graphics toolbar.

Material

1. In the Model Builder window, under Model 1 right-click Materials and choose Add Material.

2. Pick Topas from the Materials Library.

3. Select Domains 1 and 4 only. All domains are selected by default. PML will be of topas.

4. In the Material settings window, click to expand the Material Properties section.

5. In the Material properties tree, select Electromagnetic Models>Refractive Index>Refractive index (n).

6. Click Add to Material.

7. In the Model Builder window, expand the Material 1 node, then click Refractive index.

8. In the Property Material window, locate the Material Contents section.

ELECTROMAGNTIC WAVES, FREQUENCY DOMAIN

Wave Equation, Electric 1

1. In the Model Builder window, expand the Model 1>Electromagnetic Waves, Frequency Domain node, then click Wave Equation, Electric 1.

2. In the Wave Equation, Electric settings window, locate the Electric Displacement Field section.

3. From the Electric displacement field model list, choose Refractive index.

4. Choose Refractive Index> from material.

MESH 1

The default mesh settings aim for a good resolution of all curved boundaries. In this model, they would lead to a high number of elements. By relaxing the growth rate and the curvature resolution requirement, you can get a decently accurate solution with fewer elements.

Size

The default mesh settings aim for a good resolution of all curved boundaries. In this model, they would lead to a high number of elements. By relaxing the growth rate and the curvature resolution requirement, you can get a decently accurate solution with fewer elements.

1. In the Model Builder window, under Model 1 right-click Mesh 1 and choose Physics Controlled Mesh.

2. In the Element Size box, choose Finer. A finer element size results in more accurate solution but longer computational time.

A.2 STUDY

1. In the Study 1 window, go to Step 1: Mode Analysis.

2. In the Mode Analysis window, type desired number of modes as any number between 10 to 20

3. Choose Transform> Effective Mode Index.

4. Choose Search for modes around> 1.2.

5. Put mode analysis frequency equal to f;

6. In the Study 1 Node, click Compute. A.3 RESULTS

Electric field

The default plot shows the distribution of the electric field norm for the lowest of the frequencies. Because this is below the cutoff frequency of the waveguide, the wave does not propagate through the outlined guide geometry.

1. In the Model Builder window, under Results click Electric field.

2 .Choose an Effective Index value to see its distribution.

4. Click the Plot button.

5. In the Model Builder window, expand the Electric field node, then click Surface.

6. In the Electric Field Node, Right Click & choose arrow surface. In the Arrow Surface window, find the coloring & style subsection & choose the Arrow Length as Normalized. This helps to visualize the polarization of the LP mode.

7. For nonlinearity, go Results> Derived Values> Integration> Surface Integration.

8. Under Surface Integration Window, select All Domains. In the expression field write $(emw.normE)^4$ & click Evaluate. Take values for the Confined modes only.

9. Go to derived values & take another surface integration. In the expression field write $(emw.normE)^2$ & click Evaluate.

10. Square the result found in step 9 & divide by the result in step 8. Multiply by 1e12 to find the effective mode area in μm^2.

Appendix B
Basic Math lab Codes

V parameter:

```
clc
clear all
Dcore =;  %put in Dcore value
f = 0.3:0.02:2; %put in frequency range
n = [];     %put in real part of refractive index
b = 10^12.*f;

lambda(:,:,1)=0;
for x=1:length(f)
   lambda(x) = (3*10^8/(b(x)));
end
v(:,:,1) = 0;

for x=1:length(f)
   v(x) = ((2*pi*Dcore/2)/lambda(x))*sqrt((n(x)^2)-1);
end

plot(f,v);
```

Confinement loss:

```
clear all
clc

c = 3*10^8;
f = 10^12;
lambda = c/f;
Dcore = 200:5:400;

ni = abs([]);   %put in imaginary part of refractive index
alpha_cl1 = ((8.686*2*pi)/(lambda*4.34*100)).*ni;
plot(Dcore,alpha_cl1);
```

EML:

```
clc
clear all
% f = 1 THz
Dcore = 200:5:280;  %put in core diameter range

alpha_eff1 = 0.2.*[];
plot(Dcore,[alpha_eff1]);
```

Power Fraction:

```
clc
clear all
f = 0.3:0.02:2;     %put in frequency range
pf_aircore = 100*[];    %put in power fraction in air core

pf_solid = 100*[];      %put in power fraction in solid mat

pf_clad = 100*[];       %put in power fraction in cladding air

plot(f,[pf_aircore,pf_solid,pf_clad]);
```

References

[1] M. Y. Frankel, S. Gupta, J. A. Valdmanis and G. A. Mourou, “Terahertz attenuation and dispersion characteristics of coplanar transmission-lines,” IEEE Trans. Microwave Theory Tech., MTT-39, no.6, pp.910-916, 1991.

[2] Federica Poli, AnnamariaCucinotta, Stefano Selleri, Photonic Crystal Fibers.

[3] Govind P. Agrawal, Nonlinear Fiber Optics, Fourth Edition

[4] Dr.Zeba Rahman Siddiqui, Dr.Pratima Srivastava, Dr.ShivamYadav , Dr.Robin Srivastava , Dr.Zia Arshad Khan, “A Review- Basic of Laser and Its Role in Periodontics: Part I” IOSR Journal of Dental and Medical Sciences (IOSR-JDMS) e-ISSN: 2279-0853, p-ISSN: 2279-0861.Volume 14, Issue 12 Ver. V (Dec. 2015), PP 45-52

[5] S. G. Leon-Saval, T. A. Birks, W. J. Wadsworth and P. St. J. Russell, “Supercontinuum Generation in submicron fiber waveguides,” Opt. Exp., vol. 12, no. 13, pp. 2864-2869, June2004.

[6] T. G. Euser, J. S. Y. Chen, M. Scharrer, P. St. J. Russell, N. J. Farrer, and P. J. Sadler, “Quantitative broadband chemical sensing in air-suspended solid-core fibers,” J. Appl. Phys.,vol. 103, pp. 103-108, 2008.

[7] L. Dong, B. K. Thomas, and L. Fu, “Highly nonlinear silica suspended core fibers,” Opt. Exp., vol. 16, no. 21, pp. 16423-16430, Oct. 2008.

[8] J. C. Knight, “Photonic crystal fibers and fiber lasers”, Vol. 24, No. 8/ August 2007/ J. Opt. Soc. Am. B

[9] R. Buczynski, “Photonic Crystal Fibers”, Vol. 106 (2004) ACTA PHYSICA POLONICA A No.2.

[10] Z. Chen, L. Yuan, G. Hefferman and T. Wei, "Terahertz Fiber Bragg Grating for Distributed Sensing," in IEEE Photonics Technology Letters, vol. 27, no. 10, pp. 1084-1087, May15, 15 2015.

[11] Federica Poli, AnnamariaCucinotta, Stefano Selleri, Photonic Crystal Fibers.

[12] E.J. Nichols and J.D. Tear, “joining the infrared and electric wave spectra”, Astrophys. J., vol.61,pp 17-37,1925.

[13] J. Johny, T. Smith, K. Bhavs.ar and R. Prabhu, "Design of optical fibre based highly sensitive acoustic sensor for underwater applications," OCEANS 2017 - Aberdeen, Aberdeen, 2017,pp.1-5. doi: 10.1109/OCEANSE.2017.8084974

[14] E. Grossman, private communiucation.

[15] V. Petrov, A. Pyattaev, D. Moltchanov and Y. Koucheryavy, "Terahertz band communications: Applications, research challenges, and standardization activities," 2016 8th

International Congress on Ultra-Modern Telecommunications and Control Systems and Workshops (ICUMT), Lisbon, 2016, pp. 183-190.
[16] R. H. Jacobsen, D. M. Mittleman, and M. C. Nuss, "Chemical recognition of gases and gas mixtures with terahertz waves," Optics Lett., vol. 21, no.24, pp. 2011-2013, 1996.
[17] Q. Chen, Z. Jiang, G. X. Xu, and X. C. Zhang, "Near-field terahertz imaging with a dynamic aperture," Optics Lett., vol. 25, no.15, pp.1122-1124, 2000.
[18] Mittleman DM, Hunsche S, Boivin L, Nuss MC. T-ray tomography. Opt Lett. 1997;22:904–906.
[19] Beard MC, Turner GM, Schmuttenmaer CA. Subpicosecond carrier dynamics in low-temperature grown. GaAs as measured by time-resolved terahertz spectroscopy. J Appl Phys. 2001;90:5915–5923..
[20] G. L. Carr, M. C. Martine, W. R. McKinney, K. Jordan, G. R. Neil, and G. P. Williams, "Very high power THz radiation at Jefferson Lab," in Physics in Medicine and Biology, vol 47, pp 3761-3764.
[21] V. Petrov, D. Moltchanov, and Y. Koucheryavy, "Applicability assessment of terahertz information showers for next-generation wireless networks," in 2016 IEEE International Conference on Communications (ICC), pp. 1–7, May 2016.
[22] "Imt Vision towards 2020 and Beyond." https://www.itu.int/dmspub/itur/oth/0a/06/R0A0600005D0001PDFE.pdf. Accessed: 2016-0818.
[23] I. Kallfass, F. Boes, T. Messinger, J. Antes, A. Inam, U. Lewark, A. Tessmann, and R. Henneberger, "64 gbit/s transmission over 850 m fixed wireless link at 240 ghz carrier frequency," Journal of Infrared, Millimeter, and Terahertz Waves, vol. 36, no. 2, pp. 221–233, 2015.
[24] A. Hirata, T. Kosugi, H. Takahashi, R. Yamaguchi, F. Nakajima, T. Furuta, H. Ito, H. Sugahara, Y. Sato, and T. Nagatsuma, "120-GHz-band millimeter-wave photonic wireless link for 10-Gb/s data transmission," IEEE Transactions on Microwave Theory and Techniques, vol. 54, no. 5, pp. 1937–1944, 2006.
[25] I. F. Akyildiz and J. M. Jornet, "Realizing ultra-massive {MIMO} communication in the (0.0610) terahertz band," Nano Communication Networks, vol. 8, pp. 46 – 54, 2016. Electromagnetic Communication in Nano-scale.
[26] A. Volkova, D. Moltchanov, V. Petrov, and Y. Koucheryavy, "Joint cooling and information transmission for board-to-board communications," in Proceedings of the Second Annual International Conference on Nanoscale Computing and Communication, NANOCOM' 15, (New York, NY, USA), pp. 32:1–32:6, ACM, 2015.
[27] J. Israel, J. Martinovic, A. Fischer, M. Jenning, and L. Landau, "Optimal antenna positioning for wireless board-to-board communication using a butler matrix beamforming

network," in Smart Antennas (WSA), 2013 17th International ITG Workshop on, pp. 1–7, March 2013.

[28] https://www.compadre.org/informal/features/featureSummary.cfm?FID=402

[29] N. Chen, J. Liang, and L. Ren, "High birefringence, low-loss porous fiber for single-mode terahertz-wave guidance," Appl. Opt., vol. 52, no. 21, pp. 5297-5302, 2013.

[30] D. Moltchanov, A. Antonov, A. Kluchev, K. Borunova, P. Kustarev, V. Petrov, Y. Koucheryavy, and A. Platunov, "Statistical traffic properties and model inference for shared cache interface in multi-core cpus," IEEE Access, vol. PP, no. 99, pp. 1–1, 2016.

[31] Berenger, J., "A perfectly matched layer for the absorption of electromagnetic waves," Journal of Computational Physics, vol. 114, no. 2, pp. 185–200, 1994.

[32] M. Born and E. Wolf, Principles of Optics, 7th ed., Cambridge University Press, New York, 1999.

[33] G.P.Agrawal, "Nonlinear Fiber Optics", Fourth Edition

[34] John M. Senior, "Optical Fiber Communications", Third edition

[35] Rei Kitamura, Laurent Pilon, and MiroslawJonasz, "Optical constants of silica glass from extreme ultraviolet to far infrared at near room temperature," Appl. Opt. 46, 8118-8133 (2007)

[36] G.P.Agrawal, "Fiber-Optic Communication Systems", Fourth Edition.

[37] N.A. Mortensen, J.R. Folkenberg, M.D. Nielsen, K.P. Hansen, Modal cut-off and the Vparameter in photonic crystal fibers, Opt. Lett. 28 (2003) 1879–1881.

[38] L. G. Cohen, C. Lin, and W. G. French, Electron. Lett. 15, 334 (1979).

[39] L. G. Cohen, W. L. Mammel, and S. Lumish, Opt. Lett. 7, 183 (1982).

[40] S. J. Jang, L. G. Cohen, W. L. Mammel, and M. A. Shaifi, Bell Syst. Tech. J. 61, 385 (1982).

[41] V. A. Bhagavatula, M. S. Spotz, W. F. Love, and D. B. Keck, Electron. Lett. 19, 317 (1983).

[42] https://www.rp-photonics.com/

[43] M. B. Byrne et al., "Simultaneous measurement of orthogonal components of polarization in a free-space propagating terahertz signal using electro-optic detection," Appl. Phys. Lett., vol. 98, no. 15, pp. 151104, 2011.

[44] N. Karpowicz et al., "Coherent heterodyne time-domain spectrometry covering the entire "terahertz gap"," Appl. Phys. Lett., vol. 92, no. 1, pp. 011131, 2008.

[45] S. E. Kim et al., “Elliptical defected core photonic crystal fiber with high birefringence and negative flattened dispersion,” Opt. Express, vol. 20, no. 2, pp. 1385-1391, 2012.

[46] Y. Yue et al., “Highly birefringent elliptical-hole photonic crystal fiber with squeezed hexagonal lattice,” Opt. Lett., vol. 32, no. 5, pp. 469–471, 2007.

[47] H. B. Chen et al., “Squeezed lattice elliptical hole terahertz fiber with high birefringence,” Appl. Opt., vol. 48, no. 20, pp. 3943–3947, 2009.

[48] S. Atakaramians et al., “Low loss, low dispersion and highly birefringent terahertz porous fibers,” Opt. Commun., vol. 282, no. 1, pp. 36–38, 2009.

[49] S. Atakaramians, et al., “THz porous fibers: Design, fabrication and experimental characterization,” Opt. Express, vol. 17, no. 16, pp. 14053– 15062, 2009.

[50] K.-H. Tsai, K.-S. Kim, and T. F. Morse, “General solution for stressinduced polarization in optical fibers,” J. Lightwave Technol., vol. 9, pp. 7–17, Jan. 1991.

[51] K. Tajima and Y. Sasaki, “Transmission loss of a 125 m diameter PANDA fiber with circular stress-applying parts,” J. Lightwave Technol., vol. 7, pp. 674–679, Apr. 1989.

[52] G. P. Agrawal, Fiber-Optic Communications Systems. New York: Wiley, 1997.

[53] Kurokawa, K., Tajima, K., Tsujikawa, K., and Nakajima, K., “Reducing the losses in photonic crystal fibres,” in Proc. European Conference on Optical Communication ECOC 2005, Glasgow, Scotland, Sept. 25–29, 2005.

[54] K. Nielsen, H.K. Rasmussen, P.U. Jepsen, O. Bang, Porous-core honeycombbandgap THz fiber, Opt. Lett. 36 (5) (2011) 666–668.

[55] H. Bao, K. Nielsen, H.K. Rasmussen, P.U. Jepsen, Fabrication and characterization of porous-core honeycomb bandgap THz fibers, Opt. Express 20 (28) (2012) 29507–29517.

[56] M. Uthman, B.M.A. Rahman, N. Kejalakshmy, A. Agarwal, K.T.V. Grattan, Design and characterization of low-loss photonic crystal fiber, IEEE photonics J. 4 (6) (2012).

[57] S.F. Kaijage, Z. Ouyang, X. Jin, Porous core photonic crystal fiber for low lossterahertz wave guiding, IEEE Photonics Technol. Lett. 25 (15) (2013).

[58] Hansen, K.P., Jensen, J.R., Jacobsen, C., Simonsen, H.R., Broeng, J.,Skovgaard, P.M.W.,Peterson, A., and Bjarklev, A., "Highly Nonlinear photonic crystal fiber with zero-Dispersion at 1.55 IJm," OFC'02, Post deadline, 2002.

[59] Nielsen, M.D., Mortensen, N.A., and Folkenberg, J.R., "Reduced microdeformation attenuation in large-mode area photonic crystal fibers for visible applications," Opt. Lett., vol.28, pp. 1645, 2003b.

[60] Finazzi, V., Monro, T.M., and Richardson, D.J., "The role of confinement loss in highly nonlinear silica holey fibers," IEEE Photon. Technol. Lett., vol.15, no.9, pp.1246-1248, 2003.

[61] Knight, J.C., Birks T. A., Russell, P. st. J., and de Sandro, J-P, "Properties of photonic crystal fiber and the effective index model," J. Opt. Soc. Am. A-Optics Image Science and Vision, vol. 15, pp. 748-752, 1998c.

[62] T.K. Revathi, K. Sunilkumar, A. Robert, Design and simulation of very low confinement loss photonic crystal fiber for bio-sensing, in: International Conference on Computing and Control Engineering, India, 2012, p. 541.

[63] J. Sakai, H. Niiro, Confinement loss evaluation based on a multilayer division method in Bragg fibers, Opt. Express 16 (2008) 1885–1902.

[64] V. Finazzi, T.M. Monro, D.J. Richardson, The Role of Confinement Loss in Highly Nonlinear Silica Holey Fibers, IEEE Photon. Technol. Lett. 15 (2003) 1246–1248.

[65] Williamson, C., "Holey fibers!" Light Reading- Networking the Telecom Industry, Nov 21, 2002.

[66] K. Wang and D. M. Mittleman, “Metal wires for terahertz wave guiding,” Nature, vol. 432, no. 7015, pp. 376–379, 2004.

[67] B. Bowden, J. A. Harrington, and O. Mitrofanov, “Silver/polystyrene coated hollow glass waveguides for the transmission of Terahertz radiation,” Opt. Lett., vol. 32, no. 20, pp. 2945–2947, 2007

[68] L.-J. Chen, H.-W. Chen, T.-F. Kao, J.-Y. Lu, and C.-K. Sun, “Lowloss subwavelength plastic fiber for terahertz waveguiding.,” Opt. Lett., vol. 31, no. 3, pp. 308–310, 2006.

[69] K. Nielsen, H. K. Rasmussen, A. J. Adam, P. C. Planken, O. Bang, and P. U. Jepsen, “Bendable, low-loss Topas fibers for the terahertz frequency range,” Opt. Express, vol. 17, no. 10, pp. 8592–8601, 2009.

[70] W. Yuan, L. Khan, D. J. Webb, K. Kalli, H. K. Rasmussen, A. Stefani, and O. Bang, “Humidity insensitive TOPAS polymer fiber Bragg grating sensor.,” Opt. Express, vol. 19, no. 20, pp. 19731– 19739, 2011.

[71] C. Markos, A. Stefani, K. Nielsen, H. K. Rasmussen, W. Yuan, and O. Bang, “High-Tg TOPAS microstructured polymer optical fiber for fiber Bragg grating strain sensing at 110 degrees.,” Opt. Express, vol. 21, no. 4, pp. 4758–4765, 2013.